A ^{95}Mo Solid-State NMR Study of Hydrodesulfurization Catalysts. 1. Formation of Fresh HDS Catalyst Precursors by Adsorption of Polyoxomolybdates onto γ-Alumina

John C. Edwards, Richard D. Adams,* and Paul D. Ellis*

Contribution from the Department of Chemistry, University of South Carolina, Columbia, South Carolina 29208. *Received November 6, 1989*

Abstract: The solid-state ^{95}Mo NMR of oxomolybdates and polyoxomolybdates adsorbed to γ-alumina was utilized to characterize the molybdenum species present at circa monolayer coverages of molybdenum. This represents the first attempt at using solid-state NMR to look directly at the molybdenum species on the surface of "fresh" hydrodesulfurization catalyst precursors. The selectively excited central $\pm^1/_2$ transition line shapes were obtained, by the solid-echo technique, for several polyoxomolybdates, which are considered model compounds of the surface molybdena species, as well as for the uncalcined and calcined catalysts at various loadings. The spectra were obtained for static and magic angle spinning samples. Static sample spectra of the catalysts reveal inhomogenously broadened lines owing to a range of surface species being present. Magic angle spinning spectra show the presence of four possible species on the surface of the uncalcined catalysts and two possible species present on the surface of calcined catalysts. Spikelet echo spectra identified static adsorbed species [speculated to be predominantly adsorbed tetrahedral/octahedral molybdena, and perhaps $Al_2(MoO_4)_3$], and a dynamic species (speculated to be disordered, surface-interactive tetrahedral and octahedral molybdates), in the uncalcined catalyst samples. Upon calcination the line widths of the static and MAS spectra are increased, indicating a polymerization of the surface species to form a MoO_3-like phase. The spikelet echo spectra reveal the loss of the dynamic species upon calcination, indicating that it is adsorbed to the surface or polymerized with the molybdenum surface species. The $Al_2(MoO_4)_3$ phase is stable to calcination and also appears in the calcined catalysts. These qualitative speculations are in close agreement with the results of other researchers using other characterization techniques. An interactive graphical curve-fitting program was used to calculate, from the various line shapes, the values of the quadrupolar coupling constant, the asymmetry parameter of the electric field gradient, the three principal values of the chemical shielding tensor, and the three Euler angles that relate the noncoincident quadrupole and chemical shielding principal axis systems. Assignments of the quadrupole tensors to the different sites present in the model species were made based on the relationship between the Q_{cc} value and molecular distortion of the octahedral sites. These results have shown the feasibility of using solid-state ^{95}Mo NMR to investigate heterogeneous and homogeneous catalysts containing active molybdenum species.

Introduction

Catalysts prepared by the impregnation of γ-Al_2O_3 with a solution of ammonium heptamolybdate have been the subject of many investigations due to the importance of MoO_x-γ-Al_2O_3 as an oxidation catalyst, as well as being involved in olefin metathesis and hydrogenation catalysts. We will be studying, in this case, molybdena/alumina catalysts in the context of them being the precursors to hydrodesulfurization (HDS)[1-8] and hydrodenitrogenation (HDN)[9] catalysts. HDS catalysts are used industrially to remove sulfur from petroleum feedstocks and coal by its conversion to H_2S and hydrocarbon products. The commercial catalysts consist of either molybdenum or tungsten, promoted by either nickel or cobalt, supported on γ-alumina, and are usually prepared by incipient wetness impregnation with an ammonium heptamolybdate solution, (i.e., by filling only the pore volume of the alumina). The "fresh" catalyst is reduced and sulfided to form the active catalyst, which is the subject of ongoing research in our laboratory, the results of which will be dealt with in future publications. We present here the results of our endeavors to characterize the oxomolybdenum surface species present on the γ-alumina surface of the fresh molybdena catalyst. To date, a variety of spectroscopic techniques have been used in attempts to characterize the interaction between the molybdenum species and the alumina support. XPS,[10-12] γ-ray dispersion,[13] Raman[10,14-20] and IR[21,22] spectroscopy, NO/CO_2 chemisorption,[23] and UV-vis reflectance[14,16,22] have provided the best information on the molecular nature of molybdena on alumina, but there is still disagreement as to the mechanism by which the heptamolybdate anions present in the impregnation solution are adsorbed onto the alumina surface. It has been suggested by Wang and Hall[14] that the heptamolybdate species, present in solutions with low initial pH, are adsorbed intact during impregnation to give a supported heptameric species. This adsorption occurs due to an electrostatic attraction between the positively charged alumina surface (at a pH lower than the isoelectric point) and the polyoxomolybdate anion. It is thought that these supported clusters are stable even after calcination. Another possibility, put forward by Knözinger and Jeziorowski,[16] is that exchange of $[MoO_4]^{2-}$ with the surface hydroxyl groups increases the pH at the surface, which in turn causes the dissociation of the heptameric species to the monomer, $[MoO_4]^{2-}$. Thus, islands of tetrahedral molybdate are formed on the alumina surface. Upon calcination

(1) Schuman, S. C.; Shalit, H. *Catal. Rev.* **1970**, *4*, 245.
(2) Weisser, O.; Landa, S. In *Sulphide Catalysts. Their Properties and Applications*; Pergamon: Oxford, 1973.
(3) Amberg, C. H. *J. Less-Common Met.* **1974**, *36*, 339.
(4) Grange, P.; Delmon, B. *J. Less-Common Met.* **1974**, *36*, 353.
(5) de Beer, V. H. J.; Schuit, G. C. A. In *Preparation of Catalysts*; Delmon, B., Jacobs, P. A., Poncelet, G., Eds.; Elsevier: Amsterdam, 1976; p 343.
(6) Ohtsuka, T. *Catal. Rev.—Sci. Eng.* **1977**, *16*, 291.
(7) Gates, B. C.; Katzer, J. R.; Schuit, G. C. A. In *Chemistry of Catalytic Processes*; McGraw-Hill: New York, 1979; p 390.
(8) Grange, P. *Catal. Rev.* **1980**, *21*, 135.
(9) Ho, T. C. *Catal. Rev.—Sci. Eng.* **1988**, *30*, 117.
(10) Zingg, D. S.; Makovsky, L. E.; Tischer, R. E.; Brown, F. R.; Hercules, D. M. *J. Phys. Chem.* **1980**, *84*, 2899.
(11) Clausen, B. S.; Lengeler, B.; Topsøe, H. *Polyhedron* **1987**, *5*, 199.
(12) Hayden, T. F.; Dumesic, J. A. *J. Catal.* **1987**, *103*, 366.
(13) Butz, T.; Vogdt, C.; Lerf, A.; Knözinger, H. *J. Catal.* **1989**, *116*, 31.
(14) Wang, L.; Hall, W. K. *J. Catal.* **1980**, *66*, 251; **1982**, *77*, 232; **1983**, *83*, 242.
(15) Knözinger, H.; Jeziorowski, H. *J. Phys. Chem.* **1978**, *82*, 2002.
(16) Knözinger, H.; Jeziorowski, H. *J. Phys. Chem.* **1979**, *83*, 1166.
(17) Cheng, C. P.; Schrader, G. L. *J. Catal.* **1979**, *60*, 276.
(18) Brown, F. R.; Makovsky, L. E.; Rhee, K. H. *J. Catal.* **1977**, *50*, 162.
(19) Brown, F. R.; Makovsky, L. E.; Rhee, K. H. *J. Catal.* **1977**, *50*, 385.
(20) Kasztelan, S.; Payen, E.; Toulhoat, H.; Grimblot, J.; Bonnelle, J. P. *Polyhedron* **1987**, *5*, 157.
(21) Millman, W. S.; Segawa, K.; Smrz, D.; Hall, K. W. *Polyhedron* **1987**, *5*, 169.
(22) Giordano, N.; Bart, J. C. J.; Vaghi, A.; Castellen, A.; Martinotti, G. *J. Catal.* **1975**, *36*, 81.
(23) O'Young, C.-L.; Yang, C.-H.; DeCanio, S. J.; Patel, M. S.; Storm, D. A. *J. Catal.* **1988**, *113*, 307.

0002-7863/90/1512-8349$02.50/0

deamination occurs, followed by a condensation of the resulting molybdic acid with the surface hydroxyls, to form a polymeric oxomolybdenum species. According to Medema et al.,[24] bulk MoO_3 is always formed at higher loadings and a "subsurface" $Al_2(MoO_4)_3$ phase was also detected in some catalysts. This $Al_2(MoO_4)_3$ phase was also detected by McMillan et al.[25] by solid-state magic angle spinning ^{27}Al NMR, although our attempts to repeat that experiment yielded no sign of this phase. It has been shown that in cases of high pH (>8.5), the negatively charged environment of the alumina surface resists adsorption of the molybdate anions present in solution. As the impregnation slurry dries, the bulk of the molybdate is unadsorbed and precipitates onto the surface of the alumina. During calcination these precipitates then form "free" MoO_3 crystallites.[14]

^{95}Mo liquid-state NMR has been used to investigate the interaction of molybdates with alumina.[26,27] These involved the characterization of the molybdate solutions present in the pores of γ-alumina. Both studies found that the equilibrium between the heptamolybdate and molybdate species was greatly displaced to the molybdate inside the γ-alumina pores. Does this mean that the heptamolybdate is preferentially adsorbed, leaving only the molybdate present in solution to be observed, or alternatively, is the heptamolybdate dissociating to the molybdate due to an increase in the pH at the surface of the alumina, caused by a preferential exchange of molybdate with the hydroxyl groups of the alumina, which causes an increase in the concentration of $[MoO_4]^{2-}$ in the pores? There is evidence for both adsorption mechanisms and it is probably a combination of the two.

In an effort to answer these questions we have used ^{95}Mo solid-state NMR to examine the catalyst with various loadings of molybdenum (3%, 6%, 8%, 12%, 16%, and 24% wt/wt at a pH of 5.2 for the impregnation solution). It is estimated that a loading of ~16% is the equivalent of a monolayer coverage of the surface. A sample of the 8% loading was investigated by using an impregnation solution of pH 8.2. The effect of pH on the species present on the surface was also investigated in the case of the 12% loading catalyst, in which samples were prepared with impregnation solutions at pH 2.0, 5.2, and 9.0. The catalysts were observed in their uncalcined and calcined states. Various model compounds such as $Mo(CO)_6$, $Na_2MoO_4 \cdot 2H_2O$, $(NH_4)_6Mo_7O_{24} \cdot 4H_2O$, MoO_3, Al_2MoO_4, $PbMoO_4$, $(NH_4)_2Mo_2O_7$, $[Mo_6O_{19}]^{2-}$, and $[Mo_8O_{26}]^{4-}$ were also investigated.

^{95}Mo is a quadrupolar nucleus with a nuclear spin of $^5/_2$ and a relatively high natural abundance of 15.8%. It has a comparatively small quadrupole moment, Q, of 0.12×10^{-24} cm^2, which means that the line shapes in the solid state are, generally, not too broad. The signal-to-noise ratio has been enhanced by using 94.9% ^{95}Mo enriched ammonium heptamolybdate for the impregnation of the alumina.

Static powder and magic angle spinning (MAS) spectra were obtained for each sample. For the catalyst samples, spikelet spectra[28,29] were recorded to obtain dynamical information on the species present on the surface.

Experimental Section

Materials and Impregnation Procedure. γ-Alumina was obtained from Johnson-Matthey and was found to have a surface area of 115 m^2/g when analyzed in our laboratory with a surface area analyzer made by Quanta Chrome. In reality the alumina used can be considered as a transition alumina, since γ-alumina typically has a surface area of 200–220 m^2/g. ^{95}Mo metal (94.9 atom % ^{95}Mo) was obtained from Isotec Inc. and $(NH_4)_6{}^{95}Mo_7O_{24} \cdot 4H_2O$ and $^{95}MoO_3$ were synthesized in the following manner: the molybdenum metal powder was dissolved in hot concentrated HNO_3 (Fisher Scientific), and the resulting yellow precipitate was dissolved by addition of a few milliliters of 6 M HCl. All the liquid was then evaporated and the resulting powder placed in a furnace at 800 K for 3 h, yielding $^{95}MoO_3$. The majority of the $^{95}MoO_3$ was then dissolved in a dilute NH_4OH solution and the solution pH adjusted to pH 5.2 by addition of dilute HNO_3. The $(NH_4)_6{}^{95}Mo_7O_{24} \cdot 4H_2O$ was collected after it crystallized out of solution and was characterized by laser Raman[30] and FT-IR[31] spectroscopy. Both of these characterization methods revealed the presence of small amounts of impurity, which could not be removed by further purification methods.

Mo–Al_2O_3 Catalyst Preparation. It was calculated that a 16% weight for weight loading of ammonium heptamolybdate on γ-alumina is the equivalent of a monolayer coverage. This calculation was done by assuming that the molybdenum–oxo species are adsorbed as axially coordinated $[MoO_6]$ octahedra. The area that one of these $[MoO_6]$ units occupies on the surface can then be assumed to be the area of the $Mo–O_4$ plane inherent in the octahedral structure. The area can be calculated by assuming the MoO_4 plane to be a square whose bisecting diagonal is the sum of the effective ionic *diameters* of the molybdenum cation and two oxygen anions. The effective ionic *diameters* are 1.24 Å for Mo^{6+} and 2.64 Å for O^{2-}.[32] Thus, it can be calculated that the area that each octahedral unit occupies is 21.26 Å^2. Each heptamolybdate anion can deposit seven such octahedral units onto the surface. Hence, for each heptamolybdate anion, the area of the alumina covered is 148.79 Å^2. The surface area of the γ-alumina is 115 m^2/g. In order to create a monolayer on 1 g of support one must deposit $115/1.488 \times 10^{-18}$ (i.e., 7.73×10^{19}) molecules of heptamolybdate onto the alumina surface. By comparison with Avogadro's number this equates to 1.284×10^{-4} M (0.16 g) of heptamolybdate per gram of support, i.e., 16% by weight.

The catalyst samples[33] were prepared by placing 1 g of γ-alumina in a small plastic weigh boat. The appropriate weight of ^{95}Mo-enriched hexaammonium heptamolybdate was dissolved in ~15 mL of water. In the case of the 12% loadings the solution was pH adjusted so that there were three impregnation solutions of pH 2.0, 5.2, and 9.0. For the 8% loadings two samples were prepared, one at pH 8.2 and one at pH 5.2. Then 3-mL aliquots of the solution were placed on the γ-alumina and stirred into a slurry and placed in an oven at 50 °C until dry, and the process repeated until no more solution was left. The catalyst was placed in an oven at 120 °C for 4 h. This was the uncalcined sample that was studied. The catalyst was then calcined in a furnace, under air, at 550 °C for 18 h. This was the calcined sample that was studied.

Model Species. Samples of $Na_2MoO_4 \cdot 2H_2O$ (99.5%) and $(NH_4)_2Mo_2O_7$ were obtained from Alfa Products, Morton Thiokol Inc., and were used without further purification. $Mo(CO)_6$ was also obtained from Alfa Products but was purified by sublimation before use. $(NH_4)_6{}^{95}Mo_7O_{24} \cdot 4H_2O$ was synthesized from molybdenum metal powder (94.9% ^{95}Mo from Isotec Inc.) by the method described previously for the preparation of ^{95}Mo-enriched material—$^{95}MoO_3$ was also made and collected during this synthesis. $Al_2(MoO_4)_3$ was made by calcining a 3:1 molar ratio of MoO_3 and Al_2O_3, at 750 °C for 10 h. A sample of $PbMoO_4$ was made by the reaction of a $Pb(NO_3)_2$ solution with an acidified solution (buffered at pH 4) of sodium molybdate.

The samples of $[Bu_4N]_2Mo_6O_{19}$ and $[Bu_4N]_4Mo_8O_{26}$ were obtained from the laboratory of Jon Zubieta, at the Chemistry Department of SUNY, Albany.

NMR Spectroscopy. The ^{95}Mo solid-state Fourier transform NMR spectra were obtained at 26.06 MHz on a Varian XL-400 spectrometer operating in the "wide line" mode. Static spectra were acquired by using either a broad-band tunable Doty 5-mm orthogonal powder probe or a Doty 7-mm MAS probe, both obtained from Doty Scientific (600 Clemson Rd, Columbia, SC 29223). The Doty 7-mm MAS probe was used to acquire the MAS spectra, which were taken, typically, with spinning speeds of 3.0–4.6 kHz. A broad-band tunable Doty 5-mm high-speed MAS probe was used to obtain the spectra with spin speeds greater than 5 kHz. A 30-MHz low-pass filter was utilized in order to remove any spurious signals from the transmitter rf generated by the XL-400 spectrometer. All chemical shifts are reported with respect to a 2 M Na_2MoO_4 reference solution at pH 11. The nonselective $\pi/2$ pulse width was determined from this reference solution. Typical values for this pulse width have been observed in the range of 6–9 μs. The forward power used in these experiments was typically ~576 W, while the reflected power was ~64 W. In order to selectively observe the $\pm^1/_2$ central transition we have employed the selective solid echo sequence[34–37]

(24) Medema, J.; van Stam, C.; de Beer, V. H. J.; Konings, A. J. A.; Koningsberger, D. C. *J. Catal.* **1978**, *53*, 386.
(25) McMillan, M.; Brinen, J. S.; Haller, G. L. *J. Catal.* **1986**, *97*, 243.
(26) Luthra, N. P.; Cheng, W.-C. *J. Catal.* **1987**, *107*, 154.
(27) Sarrazin, P.; Mouchel, B.; Kasztelan, S. *J. Phys. Chem.* **1989**, *93*, 904.
(28) Cheng, J. T.; Ellis, P. D. *J. Phys. Chem.* **1989**, *93*, 2549.
(29) Garroway, A. N. *J. Magn. Reson.* **1977**, *28*, 365.
(30) Tytko, K.-H.; Schönfeld, B. *Z. Naturforsch.* **1975**, *30B*, 471.
(31) Miller, F. A.; Carlson, G. A.; Bentley, F. F.; Jones, W. H. *Spectrochim. Acta* **1960**, *16*, 156.
(32) *Handbook of Chemistry and Physics*, 64th ed.; CRC Press: Boca Raton, FL, 1983–84; p F-170.
(33) The catalysts (8% and 12%, prepared at pH 5.2) were found to exhibit HDS activity consistent with kinetic data obtained on unpromoted HDS catalysts, i.e., ~9% conversion of thiophene to C_4 products, which is on the low side of average values obtained when the surface area of our catalyst is taken into consideration.
(34) Solomon, I. *Phys. Rev.* **1958**, *110*, 61.

$(\pi/2)_s-\tau_1-(\pi)_s-\tau_2$–acquire. Here the subscript s refers to a selective $\pm^1/_2$ central transition pulse. The selective pulse was obtained by dividing the nonselective $\pi/2$ pulse for the reference solution by a factor of $(I + {}^1/_2)$. These selective $(\pi/2)$ pulses were then corroborated by a pulse width array performed on the ^{95}Mo-enriched heptamolybdate sample.

In a recent note, Man and co-workers[38] alluded to a potential problem when utilizing selective pulses in quadrupolar systems. Namely, when one has a mixture of species with differing quadrupole coupling constants, one may have problems associated with the quantitative details of the experiment. This problem occurs when ω_Q (proportional to the quadrupole coupling constant) for some of the species is large compared to ω_{rf} while for others ω_Q is small relative to ω_{rf}. In this situation the rf pulse cannot be considered as selective. If one has mixed states, then the quantitation can be obtained by using a small flip angle excitation instead of selective $\pi/2$ pulses.[38] This situation is easy to diagnose with a nutation experiment.[39-47] We have performed such experiments on all of our surface precursors and have found that all of the observable ^{95}Mo is in the limit where $\omega_Q \gg \omega_{rf}$. Hence, relative quantitation via the selective echo approach is a valid method.

The static powder, selective echo spectra were obtained with the following data acquisition parameters: sweep width was 833 kHz; a 500-kHz sweepwidth was used for the static and MAS spectra of the pH-varied 12% Mo–Al_2O_3 samples; data points used were 3328 or 1472; selective pulse widths ranged from 1.4 to 1.9 μs for the 5-mm Doty probes and 2.8 to 3.1 μs for the 7-mm Doty probe. The relaxation delays used varied in the case of the model compounds from 1 to 10 s. All the catalyst spectra were obtained by using relaxation delays of 0.05 s. A 16-step phase cycle[48] was used to remove any artifacts due to imperfect pulses.

The "spikelet" experiment has been used to good effect in the past[28,29] and involves the digitization of a whole train of spin echoes. The pulse sequence is as follows: $(\pi/2)_s-\tau_1-(\pi)_s-\tau_2-[\tau-(\pi)_s-\tau]_m$. In the procedure, the magnetization is continuously sampled at the end of the first $(\pi)_s$ pulse. This leads to an induced signal, after left shifting the data to the top of the first echo, consisting of a train of refocused echoes uniformly spaced at a distance 2τ. Fourier transformation of this signal leads to a "spikelet spectrum", which would show the existence of more than one species by inconsistencies in the spikelet spacings and line widths, in that species with different T_2 times would have different spikelet line widths.

The spikelet spectra were obtained with a sweep width of 200 kHz, 3840 data points, and relaxation delay of 0.075 s. The value of m was 32, τ was 150 μs, and the receiver was blanked for 120 μs before and after each of the π pulses of the echo train. As with the solid echo experiment, a 16-step phase cycle was used.

In some of the spectra small spikes appear at chemical shifts of ~1380 and −2458 ppm (marked × on the spectra in which they appear). They were caused by a loose connection between the inductors of the 30-MHz low-pass filter. They do not appear in the chemical shift range that we are interested in and in many cases they were averaged out over time.

Line-Shape Simulation. The quadrupolar, chemical shielding parameters and the Euler angles were extracted from the model compound line shapes by simulation, using an interactive graphical curve-fitting (IGCF) program, which has been used to simulate ^{87}Rb line shapes by assuming noncoincidence of the quadrupole and chemical shielding principal axis systems (PAS).[47] The data obtained include the asymmetry parameter of the electric field gradient, η_Q, the quadrupolar coupling constant, Q_{cc}, the three principal elements of the chemical shielding tensor, σ_{11}, σ_{22}, and σ_{33}, and the Euler angles, α, β, and γ, which relate the chemical shielding PAS to the quadrupole PAS frame.

In the IGCF program the Hamiltonian used to describe the system can be written as the sum of the Zeeman, quadrupole, and chemical shielding anisotropy (CSA) terms. In our calculation, the CSA Hamiltonian has been transformed to the quadrupole PAS frame and expressed in terms of its value in the chemical shielding PAS frame. The total Hamiltonian for the system can be expressed as follows:

$$H_{system} - H_Z = H_{CS} + H_Q \tag{1}$$

where

$$H_{CS} = \frac{\omega_0 I_z \delta_{CS}}{2}\left[(3\cos^2\theta - 1)\left[\frac{(3\cos^2\beta - 1)}{2} - (\eta_{CS}/2)\sin^2\beta\cos 2\gamma\right] + \sin 2\theta\cos(\phi+\alpha)(-1.5\sin 2\beta - \eta_{CS}\sin\beta\cos\beta\cos 2\gamma) + \sin 2\theta\sin(\phi+\alpha)(\eta_{CS}\sin\beta\sin 2\gamma) + 0.5\sin^2\theta\cos(\phi+\alpha)[3\sin^2\beta - \eta_{CS}\cos 2\gamma(1+\cos^2\beta)] + 0.5\sin^2\theta\sin 2(\phi+\alpha)(2\eta_{CS}\cos\beta\sin 2\gamma)\right] \tag{2}$$

$$\delta_{CS} = \sigma_{33} - \sigma_0$$

$$\sigma_0 = {}^1/_3(\sigma_{11} + \sigma_{22} + \sigma_{33})$$

$$\eta_{CS} = (\sigma_{11} - \sigma_{22})/\delta_{CS}$$

and

$$H_Q(\pm{}^1/_2) = -(R/6\omega_0)[A(\phi)\cos^4\theta + B(\phi)\cos^2\theta + C(\phi)] \tag{3}$$

where

$$R = \omega_q^2[I(I+1) - {}^3/_4]$$

$$A(\phi) = (-27/8) - (9/4)\eta_Q\cos 2\phi - (3/8)\eta_Q^2\cos^2 2\phi$$

$$B(\phi) = (30/8) - (\eta_Q^2/2) + 2\eta_Q\cos 2\phi + (3/4)\eta_Q^2\cos^2 2\phi$$

$$C(\phi) = (-3/8) + (\eta_Q^2/3) + (\eta_Q/4)\cos 2\phi - (3/8)\eta_Q^2\cos^2 2\phi$$

$$\omega_q = 3e^2qQ/2I(2I-1)h = 3Q_{cc}/2I(2I-1)h$$

$$\eta_Q = (V_{11} - V_{22})/V_{33}$$

$$q = (1/e)V_{33}$$

The values V_{11}, V_{22}, and V_{33} are the three principal elements of the electric field gradient (EFG) tensor. The resonance frequency is denoted by ω_0 and the value η_{CS} is the asymmetry parameter of the CSA interaction. The angular values ϕ and θ are the Euler angles relating the magnetic field H_0 to the PAS frame of the quadrupole tensor.

From the spectra we have obtained it can be seen that the octahedral molybdenum sites can give rise to either broad resonances ($W_{1/2} > 10$ kHz), which remain relatively unchanged when an MAS experiment is performed, or narrow resonances ($W_{1/2}$ = 5–10 kHz), which narrow considerably upon spinning. The tetrahedral molybdenum environments also give rise to relatively narrow resonances ($W_{1/2}$ = 2–4 kHz), which narrow considerably in the MAS experiment. Using the IGCF program, we simulated pure quadrupole central $\pm^1/_2$ transition line shapes by assuming that the tetrahedral symmetry sites would yield small Q_{cc} values and low asymmetry parameters (~0.0–0.05) and the octahedral sites would yield higher Q_{cc} values and any value for the EFG asymmetry parameter from 0.0 to 1.00. For all the model compounds a complete simulation was run, which included finding the quadrupolar and, when possible, CSA parameters. For the catalyst samples, a full simulation was run only on a few of the line shapes while the rest were simulated by using only the quadrupolar parameters. In simulating the catalyst line shapes, we assumed that the line shape is caused by only one species, which brings error into the simulation as the catalyst line shapes are inhomogenously broadened; i.e., they are the superposition of several resonances caused by the various species present on the surface. The data obtained, however, do give us an idea of the average quadrupole coupling constant present.

Results

The static powder, MAS, and simulated spectra of the model compounds investigated are displayed in Figures 1–8, while the singularities and line width (at half-height $W_{1/2}$) data of these species are displayed in Table I. The static powder and MAS spectra of the catalyst samples are shown in Figures 9–13, while

(35) Weisman, I. D.; Bennett, L. H. *Phys. Rev.* **1969**, *181*, 1341.
(36) Bonera, G.; Avogadro, A.; Borsa, F. *Phys. Rev.* **1968**, *165*, 171.
(37) Warren, W. W., Jr.; Norberg, R. E. *Phys. Rev.* **1967**, *154*, 277.
(38) Man, P. P.; Klinowski, J.; Trokiner, A.; Zanni, H.; Papon, P. *Chem. Phys. Lett.* **1988**, *151*, 143.
(39) Samoson, A.; Lippmaa, E. *J. Magn. Reson.* **1988**, *79*, 255.
(40) Yannoni, C. S.; Kendrick, R. D. *J. Chem. Phys.* **1981**, *74*, 747.
(41) Man, P. P.; Theveneau, H.; Papon, P. *J. Magn. Reson.* **1985**, *64*, 271.
(42) Janssen, R.; Tijink, G. A. H.; Veeman, W. S. *J. Chem. Phys.* **1988**, *88*, 518.
(43) Geurts, F. M. M.; Kentgens, A. P. M.; Veeman, W. S. *Chem. Phys. Lett.* **1985**, *120*, 206.
(44) Samoson, A.; Lippmaa, E. *Chem. Phys. Lett.* **1983**, *100*, 205.
(45) Samoson, A.; Lippmaa, E. *Phys. Rev. B* **1983**, *28*, 6567.
(46) Kentgens, A. P. M.; Lemmens, J. J. M.; Geurts, F. M. M.; Veeman, W. S. *J. Magn. Reson.* **1987**, *71*, 62.
(47) Trokiner, A.; Man, P. P.; Thèveneau, H.; Papon, P. *Solid State Commun.* **1985**, *55*, 929.
(48) Rance, M.; Byrd, R. A. *J. Magn. Reson.* **1983**, *52*, 221.
(49) Cheng, J. T.; Edwards, J. C.; Ellis, P. D. *J. Phys. Chem.* **1990**, *94*, 553.

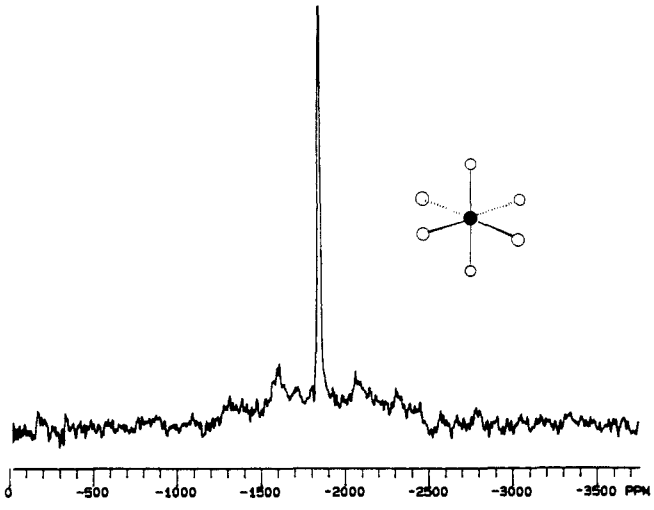

Figure 1. Selective excitation static powder spectrum of $Mo(CO)_6$, 13 300 transients, 200-Hz line broadening applied, relaxation delay of 5 s.

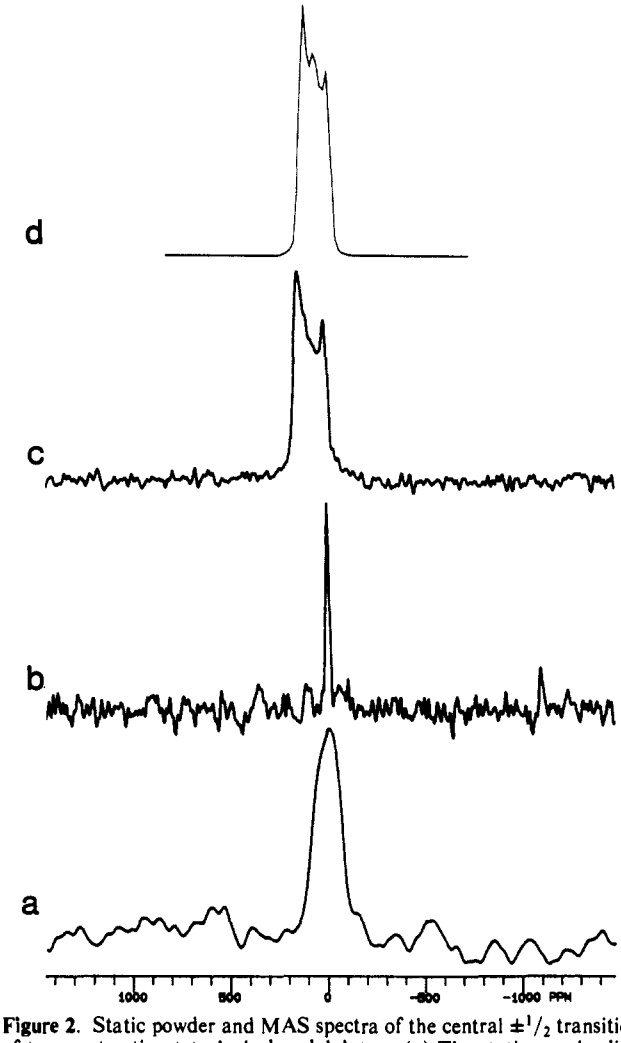

Figure 2. Static powder and MAS spectra of the central $\pm^1/_2$ transition of two contrasting tetrahedral molybdates. (a) The static powder line shape of $Na_2MoO_4 \cdot 2H_2O$, 7880 transients, relaxation delay (d1) of 5 s, 1500 Hz applied line broadening (LB). (b) The 2.9-kHz MAS of $Na_2MoO_4 \cdot 2H_2O$, 2364 transients, d1 = 5 s, LB = 200 Hz. (c) The static powder line shape of $PbMoO_4$, 5519 transients, d1 = 6 s, LB = 300 Hz. (d) The simulated line shape of $PbMoO_4$ obtained from the IGCF program.

the peak maxima positions and line-width data ($W_{1/2}$) are displayed in Table II. The values of the quadrupole and CSA parameters obtained from the IGCF program are displayed in Table III. The spikelet echo spectra are shown in Figures 14 and 15.

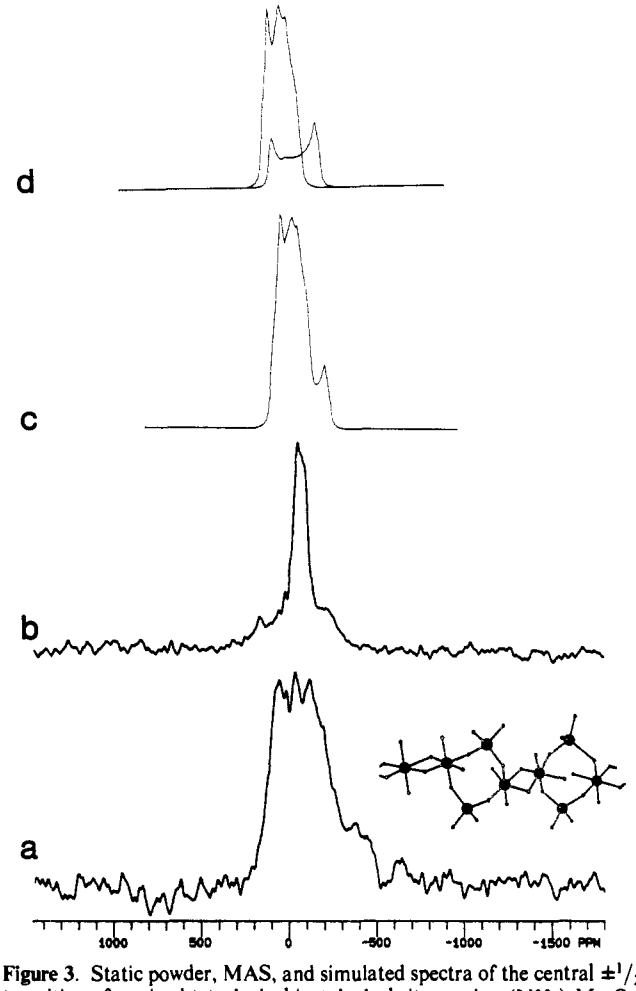

Figure 3. Static powder, MAS, and simulated spectra of the central $\pm^1/_2$ transition of a mixed tetrahedral/octahedral site species, $(NH_4)_2Mo_2O_7$. (a) Static powder spectrum, 3712 transients, d1 = 6 s, LB = 500 Hz. (b) The 4.36-kHz MAS spectrum, 3234 transients, d1 = 6 s, LB = 400 Hz. (c) The simulated spectrum obtained with the IGCF program. (d) The deconvolution of the two components of the simulated line shape. Note: The simulated spectra are not on the same scale as the experimental.

Table I. ^{95}Mo Singularity Positions and Line-Width Data Obtained on Static and MAS Powder Spectra of Molybdenum–Oxo Species

compound	spin speed, kHz	position of most intense singularity or peak max, ppm	line width ($W_{1/2}$), kHz	Figure
$Mo(CO)_6$	0	−1856	0.35	1
	1.5	−1854	0.12	
$Na_2MoO_4 \cdot 2H_2O$	0	7	3.26	2a
	2.9	4	0.34	2b
$PbMoO_4$	0	151	4.42	2c
$(NH_4)_2Mo_2O_7$	0	−36	8.99	3a
	4.4	−58	1.93	3b
MoO_3	0	−104	9.20	4a
	4.2	−114	2.34	4b
$(NH_4)_6Mo_7O_{24} \cdot 4H_2O$	0	34	13.15	5a
	4.8	4	1.84	5b
	9.0	4	1.62	5c
$(Bu_4N)_2Mo_6O_{19}$	0	505, −395	28.80	6a
	3.4	446, −289	28.70	6b
$(Bu_4N)_4Mo_8O_{26}$	0	−9		7a
	3.3	468,		7b
$H_3PMo_{12}O_{40}$	0	468, −29	57.28	8a
$Al_2(MoO_4)_3$	0	−323	3.04	8b
	3.7	−300	1.77	8c

Discussion

Investigation of Model Compounds. Although there is a growing volume of liquid-state ^{95}Mo NMR work on Mo(0), Mo(II), Mo(IV), and Mo(VI) species appearing in the literature, there is an almost complete lack of any solid-state NMR results. The

Table II. ^{95}Mo Singularity Positions and Line-Width Data Obtained for Static and MAS Powder Spectra of Calcined and Uncalcined MoO_x–Al_2O_3 Catalysts

loading catalyst state, and pH of impregnation	singularity and peak maxima positns,[a] ppm			line width ($W_{1/2}$), kHz		
	static	MAS 1	MAS 2	static	MAS 1	MAS 2
3%, uncalcn 5.2	−95			13.27		
3%, calcn, 5.2	−86			16.6		
6%, uncalcn, 5.2	−62			14.25		
6%, calcn, 5.2	−135			19.39		
8%, uncalcn, 5.2	−94			16.37		
8%, calcn, 5.2	−100			19.57		
8%, uncalcn, 8.2	−94			15.97		
8%, calcn, 8.2	−127			19.28		
12%, uncalcn, 2.0	−114	−196 (4500)	−187 (11500)	17.04	7.60	4.50
12%, calcn, 2.0	−92	−157 (4500)	−126 (12200)	20.74	6.80	5.40
12%, uncalcn, 5.2	−106	−209 (4400)	−186 (100000)	13.53	5.50	4.40
12%, calcn, 5.2	−131	−135 (4200)	−145 (11200)	19.26	7.80	6.00
12%, uncalcn, 9.0	−98	−118 (4300)	−183 (9600)	16.65	10.50	4.00
12%, calcn, 9.0	−161	−133 (4200)	−162 (10400)	16.70	12.80	5.30
16%, uncalcn, 5.2	−94			15.97		
16%, calcn, 5.2	−125			22.99		
24%, uncalcn, 5.2	−127	−203 (3000)	−193 (9600)	13.36	7.70	4.10
24%, calcn, 5.2	−109	−157 (4500)	−152 (8500)	16.47	12.5	4.10

[a] In each case the most intense singularity/peak maximum has been listed.

Table III. Estimated Values of Q_{cc} Obtained for the Oxomolybdenum Species and the Catalyst Surface Species by Simulation with the IGCF Program

catalyst or compd	Q_{cc}, MHz	η_Q	σ_{11}, ppm	σ_{22}, ppm	σ_{33}, ppm	α, deg	β, deg	γ, deg
$PbMoO_4$	2.05	0.20	−109	9	12	43	10	−56
$(NH_4)_2Mo_2O_7$ (Tet)	2.44	0.47	−35	15	51	4	79	41
$(NH_4)_2Mo_2O_7$ (Oct)	3.41	0.07	−54	7	12	0	0	0
$(NH_4)_6Mo_7O_{24}\cdot 4H_2O$								
type I	2.98	0.73						
type II	5.76	0.42						
type III	3.73	1.00						
MoO_3	3.49	0.99	18	178	349	63	70	−89
$(Bu_4N)_4Mo_8O_{26}$ (Tet)	0.00	0.34	−35	−35	10	0	0	0
$(Bu_4N)_4Mo_8O_{26}$ (Oct)	6.12	0.53	0	0	0	0	0	0
$(Bu_4N)_2Mo_6O_{19}$	4.90	0.05	35	426	445	77	0	49
loading, catalyst plate, pH								
3%, uncalcn, 5.2	3.85	0.86						
3%, calcn, 5.2	4.11	0.97						
6%, uncalcn, 5.2	3.36	0.98						
6%, calcn, 5.2	3.54	0.98	−66	−45	−38	61	20	−66
8%, uncalcn, 5.2	3.64	0.99						
8%, calcn, 5.2	4.39	0.74	−219	1	182	14	17	24
	4.48	0.83						
12%, uncalcn, 2.0	4.13	0.93						
12%, calcn, 2.0	4.26	0.77						
12%, uncalcn, 5.2	3.28	1.00						
12%, calcn, 5.2	4.13	0.89						
12%, uncalcn, 9.0	4.19	0.77						
12%, calcn, 9.0	4.29	0.80						
24%, uncalcn, 5.2	2.56	0.13	−30	37	93	14	−10	14
	4.53	0.27	−93	80	153	−11	14	−2
24%, calcn, 5.2	3.92	0.75	−30	−20	661	13	83	−6

only solid-state ^{95}Mo NMR spectra that have been published are in a study of $Mo(CO)_6$ adsorbed on alumina[50] and a few studies of molybdates.[51-53] These spectra, however, do not give one much idea of what to expect as $Mo(CO)_6$ has perfect cubic symmetry, and many molybdates have near-perfect tetrahedral symmetry. Thus, they possess only small electric field gradients, owing to the near-spherical charge distribution around the molybdenum nucleus. These small EFGs lead to narrow $\pm^1/_2$ central transition powder line shapes as shown in Figures 1 and 2a,b. In fact, the quadrupolar interaction is so small for $Mo(CO)_6$ that, in our experiment (Figure 1), the selective solid echo plainly excited the outer $\pm^3/_2$ and $\pm^5/_2$ transitions also. Thus, in an effort to lay some foundation for the catalyst study, we have obtained the spectra of several oxomolybdate species that closely model the

(50) Shirley, W. M. *Z. Phys. Chem. (Munich)* **1987**, *152*, 41.
(51) Mastikhin, V. M.; Lapina, O. B.; Maximovskaya, R. I. *Chem. Phys. Lett.* **1988**, *148*, 413.
(52) Lynch, G. F.; Segel, S. L. *Can. J. Phys.* **1972**, *50*, 567.
(53) Kautt, W. D.; Krüger, H.; Lutz, O.; Maier, H.; Nolle, A. *Z. Naturforsch.* **1976**, *31A*, 351.

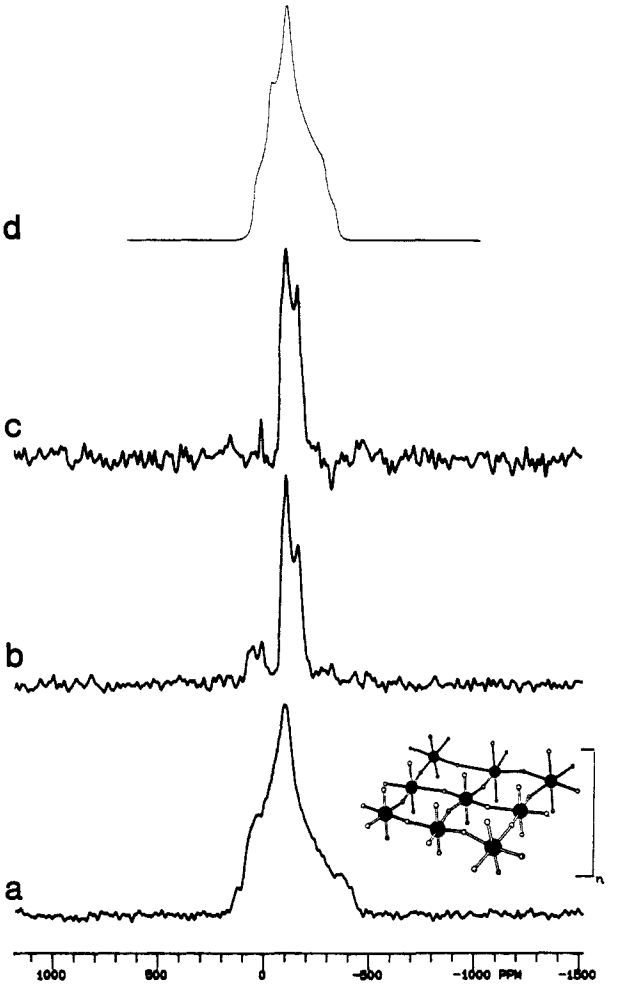

Figure 4. Static powder, MAS, and simulated spectra of the central $\pm^1/_2$ transition of octahedral MoO_3. (a) Static powder spectrum, 3338 transients, d1 = 10 s, LB = 200 Hz. (b) The 4.2-kHz MAS spectrum, 1024 transients, d1 = 7 s, LB = 200 Hz. (c) The 9.43-kHz MAS spectrum, 612 transients, d1 = 7 s, LB = 200 Hz. (d) The simulated spectrum of MoO_3 obtained with the IGCF program. Note: The simulated spectrum is not on the same scale as the experimental.

species that are claimed to be adsorbed onto the alumina surface.

In Figure 2a we have the static powder spectrum of $Na_2MoO_4{\cdot}2H_2O$, which appears to be a CSA/dipolar interaction dominated line shape of line width $W_{1/2}$ = 3.25 kHz, and a very small quadrupole contribution. When this species was examined in a 2.9-kHz MAS experiment (Figure 2b), the line shape narrowed considerably to $W_{1/2}$ = 0.34 kHz. This is to be expected as the crystal structure of $Na_2MoO_4{\cdot}2H_2O$ has shown that the molybdenum atom is in a closely tetrahedral symmetry, with Mo–O bond lengths varying from 1.75 to 1.79 Å,[54] thus leading to a small EFG at the nucleus and hence a small Q_{cc} value. Figure 2c shows the static powder spectrum of $PbMoO_4$, which is known to have a highly distorted tetrahedral molybdenum environment, leading to a much larger quadrupole contribution than is found for $Na_2MoO_4{\cdot}2H_2O$. Upon simulation with the IGCF program, the Q_{cc} was found to be 2.05 MHz and η_Q = 0.2, which is in close agreement with the values obtained by Mastikhin et al.[51] However, our line shape was a satisfactory fit only after the CSA contribution and the Euler angles exactly, as their contribution led to a reversal of the relative intensities of the two singularities observed in the simulated "quadrupole-only" line shape.

The static powder spectrum of $(NH_4)_2Mo_2O_7$ (Figure 3a) shows a two-component line shape ($W_{1/2}$ = 9 kHz) due to the presence of both distorted tetrahedral and distorted octahedral molybdenum sites, which are present in solid $(NH_4)_2Mo_2O_7$. The

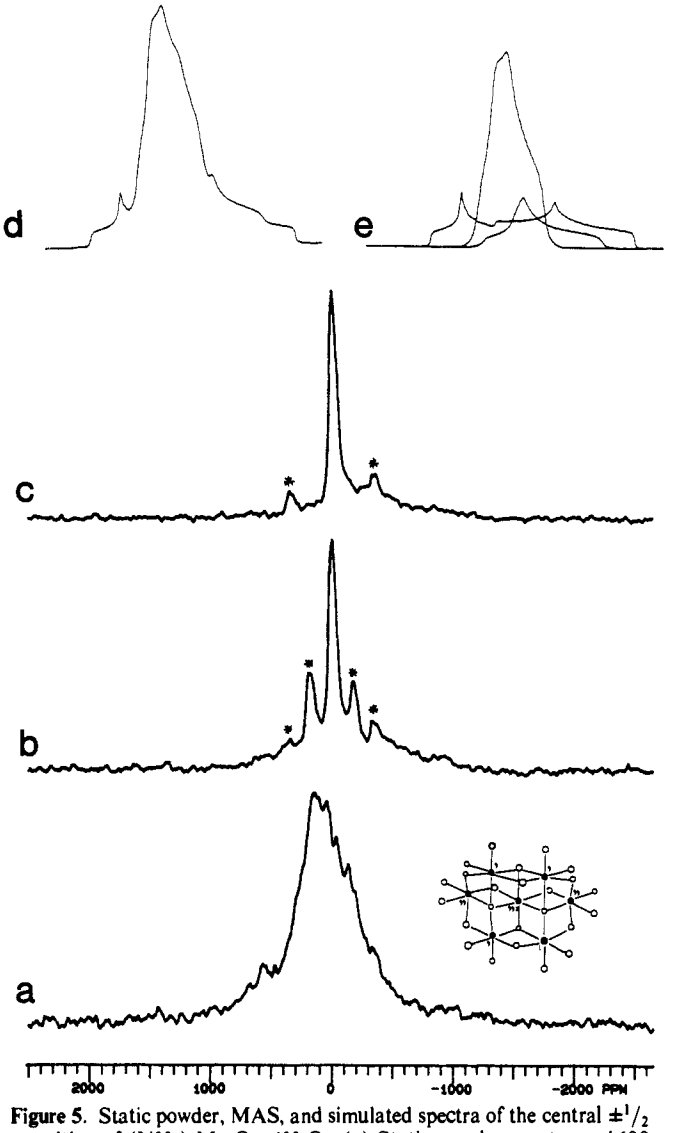

Figure 5. Static powder, MAS, and simulated spectra of the central $\pm^1/_2$ transition of $(NH_4)_6Mo_7O_{24}{\cdot}4H_2O$. (a) Static powder spectrum, 1600 transients, d1 = 2 s, LB = 500 Hz. (b) The 4.82-kHz MAS spectrum, 1600 transients, d1 = 2 s, LB = 500 Hz (* denotes spinning sidebands). (c) The 9.03-kHz MAS spectrum, 2560 transients, d1 = 2 s, LB = 500 Hz. (d) Simulated spectrum obtained with the IGCF method. (e) The deconvolution of the three components of the line shape. Note: The simulated spectra are not on the same scale as the experimental.

structure of $(NH_4)_2Mo_2O_7$ has been shown to consist of infinite chains of $[Mo_2O_7]^{2-}$ ions consisting of pairs of edge-sharing distorted octahedra linked by pairs of distorted tetrahedra.[55] In the octahedra Mo–O bond lengths range from 2.3 to 1.72 Å while in the distorted tetrahedra they range from 1.82 to 1.71 Å. Simulation of this two-component line shape (Figure 3c,d) yielded a line shape corresponding to Q_{cc} = 2.44 MHz, η_Q = 0.47, and a small value of CSA, for the tetrahedral molybdenum site. The large value of the Q_{cc} for this tetrahedral environment indicates that a high degree of distortion must be present at these sites. The octahedral site contributes a broad line to the spectrum corresponding to a quadrupole-dominated line shape with a Q_{cc} of 3.41 MHz, and η_Q = 0.07. The line due to the tetrahedral molybdenum site reduces to $W_{1/2}$ = 1.93 kHz (Figure 3b) upon performing a 4.36-kHz MAS experiment. The octahedral molybdenum resonance narrows slightly under the MAS conditions as is expected for the octahedral sites, which have lower symmetry than the tetrahedral sites, and thus give rise to larger quadrupole interactions, which are not effectively narrowed by the MAS experiment.

(54) Matsumoto, K.; Kobayashi, A.; Sasaki, Y. *Bull. Chem. Soc. Jpn.* **1975**, *48*, 1009.

(55) Armour, A. W.; Drew, M. G. B.; Mitchell, P. C. H. *J. Chem. Soc., Dalton Trans.* **1975**, 1493.

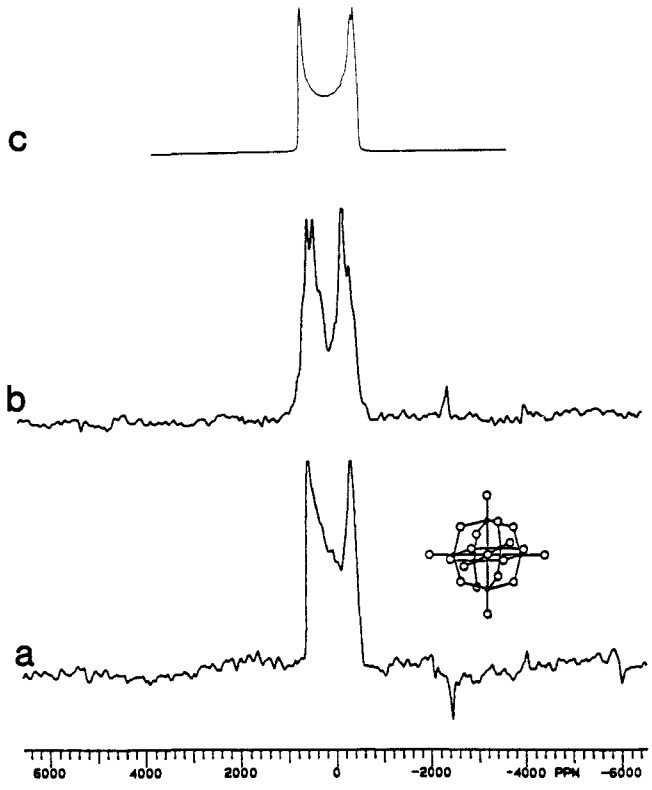

Figure 6. Static powder, MAS, and simulated spectra of the central $\pm^1/_2$ transition of an octahedral oxomolybdenum species, $[Mo_6O_{19}]^{2-}$. (a) Static powder spectrum of $(Bu_4N)_2Mo_6O_{19}$, 44 000 transients, d1 = 1 s, LB = 2000 Hz. (b) The 3.3-kHz MAS spectrum, 136 000 transients, d1 = 1 s, LB = 2000 Hz. (c) The simulated spectrum obtained from the IGCF program. Note: The simulated spectrum is not on the same scale as the experimental.

It should be pointed out here that polyoxomolybdates having octahedral symmetry tend to be distorted. This is because of the varying coordination of the oxygen atoms in the structure—some are coordinated to only one metal atom while others are coordinated to two, three, or four metal atoms. This leads to a variation in the Mo–O bond lengths from 1.7 to 2.2–2.3 Å, as well as a variation in the O–Mo–O bond angles away from the expected 90°. The angular deviation from 90° can be anywhere from 0° to ±20°. We have assumed that this distortion from the pure octahedral symmetry causes an EFG to be formed proportional to the degree of distortion, leading to large Q_{cc} values and broad line shapes. We are presently performing Gaussian 86 STO-3G calculations on several molybdenum species to prove the integrity of this assumption. Initial calculations on the effect of the various distortions on the value of Q_{cc} of a model $[MoO_6]^{6-}$ species have demonstrated that the basic assumption is correct, and these results are presented elsewhere.[56]

MoO_3 has a cubic ReO_3-type structure, which consists of $[MoO_6]$ octahedra linked by shared corners.[57] The Mo–O bond distances vary from 1.67 to 2.33 Å. It has also been suggested by Kihlborg[58,59] that MoO_3 represents a transitional stage between octahedral and tetrahedral molybdenum coordination, thus allowing one to alternatively describe MoO_3 as an infinite chain structure of tetrahedral molybdenum. It has also been shown that upon undergoing phase transitions to form the various Magnēli phases, the octahedral coordination becomes defect ridden with tetrahedral coordination predominant in and around those defects. The static powder line shape of an enriched MoO_3 sample (Figure 4a) yielded the parameters displayed in Table III upon simulation. The corresponding simulated line shape is shown in Figure 4d.

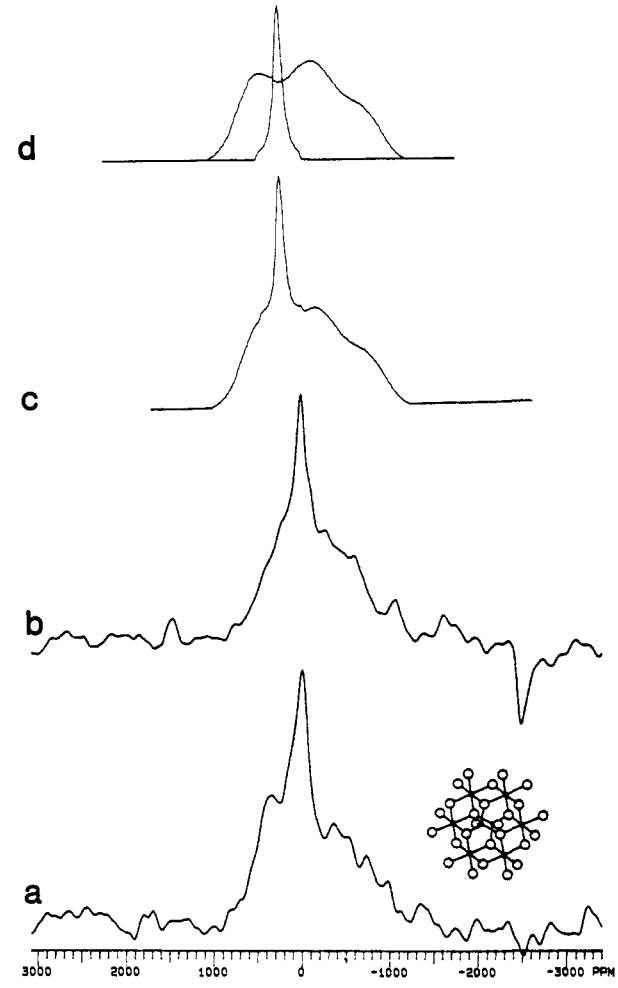

Figure 7. Static powder, MAS, and simulated spectra of the central $\pm^1/_2$ transition of a mixed octahedral/tetrahedral species containing two tetrahedral and six octahedral sites, $[Mo_8O_{26}]^{4-}$. (a) Static powder spectrum of $(Bu_4N)_4Mo_8O_{26}$, 32 400 transients, d1 = 2 s, LB = 2000 Hz. (b) The 3.4-kHz MAS spectrum, 75 000 transients, d1 = 2 s, LB = 2000 Hz. (c) The simulated spectrum obtained from the IGCF program. (d) The deconvolution of the two contributions to the line shape. Note: The simulated spectra are not on the same scale as the experimental.

The MoO_3 spectrum narrows to an appreciable extent in the MAS experiments from 5.0 to 2.3 kHz in width in the case of 4.2-kHz MAS (Figure 4b) and to 2.4 kHz in the case of 9.4-kHz MAS (Figure 4c). The maximum narrowing possible by MAS is obtained in the 4.2-kHz MAS spectrum, as the 9.4-kHz spectrum is essentially the same. There does, however, appear to be a small resonance at 4 ppm, which may be due to the presence of tetrahedral molybdenum in the bulk MoO_3. The line widths of the MAS spectra are indicative of a "slightly" distorted octahedral or a distorted tetrahedral environment for the molybdenum nuclei, thus lending some support to the seeming dual nature of the MoO_3 structure. Solid-state ^{95}Mo NMR may prove to be an effective means of quantitatively measuring the tetrahedral/octahedral coordination ratio in the various Magnēli phases that exist between MoO_3 and MoO_2 stoichiometries.

Figure 5 shows the static powder and MAS spectra of $(NH_4)_6Mo_7O_{24}{\cdot}4H_2O$. The heptamolybdate species consists of seven $[MoO_6]$ octahedra condensed together by edge sharing; the widely varying Mo–O bond lengths (1.60–2.62 Å) are due to the fact that there are oxygen atoms bonded to one, two, three, and four molybdenum atoms.[60] Crystallographically, there are seven different molybdenum sites, but structurally there are three different octahedral environments (types I–III) in the ratio 4:2:1, respectively. The three different types are shown in the structure

(56) Edwards, J. C.; Zubieta, J.; Shaikh, S. N.; Chen, Q.; Bank, S.; Ellis, P. D. *Inorg. Chem.* **1990**, *29*, 3381.
(57) Bursill, L. A. *Proc. R. Soc. London, A* **1969**, *311*, 267.
(58) Khihlborg, L. *Ark. Kem.* **1963**, *21*, 357.
(59) Kihlborg, L. *Ark. Kem.* **1963**, *21*, 471.
(60) Evans, H. T.; Gatehouse, B. M.; Leverett, P. *J. Chem. Soc., Dalton Trans.* **1975**, *505*.

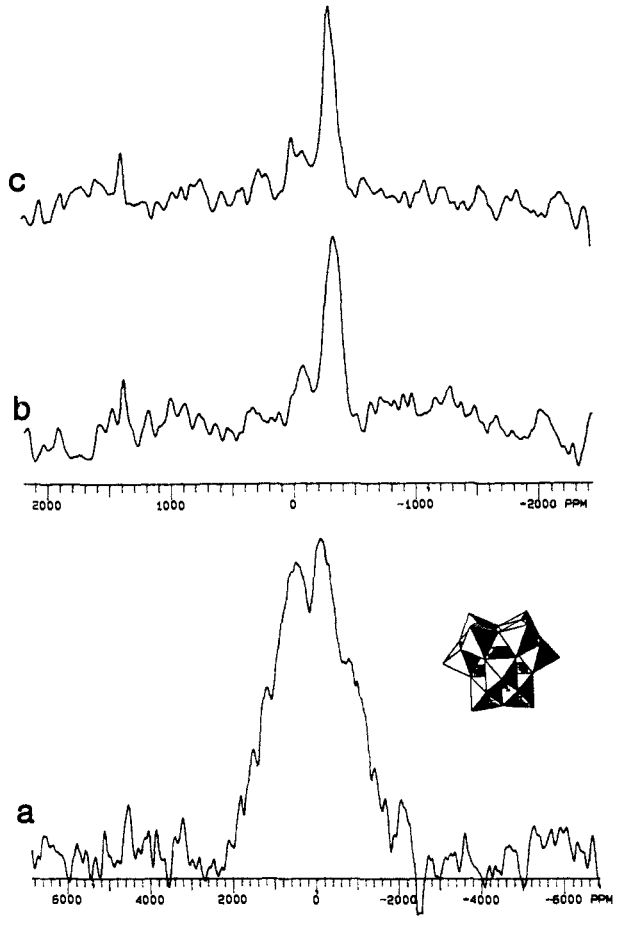

Figure 8. Static powder spectra of the central $\pm^1/_2$ transition of (a) $H_3PMo_{12}O_{40}$, 152 000 transients, d1 = 1.0 s, LB = 3000 Hz and (b) $Al_2(MoO_4)_3$, 77 000 transients, d1 = 0.5 s, LB = 1500 Hz. (c) The 3.65-kHz MAS spectrum of $Al_2(MoO_4)_3$, 132 000 transients, d1 = 0.5 s, LB = 1500 Hz.

diagram in Figure 5. Figure 5a shows the static powder spectrum, which displays a line width of 13.3 kHz and a peak maximum at 34 ppm, and shows the discontinuities that mark it as a multiple component line shape. Upon magic angle spinning at 4.82 (Figure 5b) and 9.03 kHz (Figure 5c), the line shape is split into an isotropic peak at 4 ppm, surrounded by spinning side bands. Below this resonance is a broader resonance, which is due to more distorted octahedral environments. The sideband structure of the MAS spectra indicates that the line shape is influenced by a CSA. Simulation of the static powder line shape by assuming three "quadrupole only" contributions yielded the values presented in Table III.

Investigation of the crystal structure data[60] allows one to determine the relative degrees of distortion of the different sites by calculating the average deviation of the O–Mo–O bond angles from 90° at the different sites. Type I centers have an average 9.4° deviation, type II 12.4°, and type III 10.6°, thus making the type II centers the most distorted. As we have mentioned previously, the value of Q_{cc} is proportional to the degree of distortion. This enables us to make an assignment of the quadrupole and shielding parameters obtained from the IGCF program to the three sites. We can assign the smallest Q_{cc} value (2.98 MHz) line shape to the type I sites as they are the least distorted. The line shape corresponding to a Q_{cc} value of 3.73 MHz can be assigned to the type III site, while the largest Q_{cc} value (5.76 MHz) line shape can be assigned to the most distorted site—type II. The relative intensities of the three components also support this assignment. We can now speculate upon the nature of the individual components observed in the MAS spectra. The sharp isotropic peak at 4 ppm is due to type I molybdenum centers, while the broad underlying resonance is due to types II and III, which have much larger quadrupole interactions.

Another purely octahedral species is $[Mo_6O_{19}]^{2-}$. This consists of six identical distorted octahedra condensed together by edge sharing that the molybdenum atoms of each octahedron form the vertices of another octahedron.[61] The static powder line shape (Figure 6a) corresponds to a simulated second-order quadrupole line shape (Figure 6c) with η_Q = 0.05 and Q_{cc} = 4.9 MHz, perturbed by a sizable CSA whose three principal elements are σ_{11} = 35 ppm, σ_{22} = 426 ppm, and σ_{33} = 445 ppm, α = 77°, β = 0°, and γ = 49°. The 3.4-kHz MAS spectrum of $[Mo_6O_{19}]^{2-}$ shows no appreciable narrowing of the line shape (Figure 6b). Again, a satisfactory fit between simulation and experimental could only be achieved by inclusion of the Euler angles in the calculation. Their effect was to bring about the decrease in intensity of the singularity at −395 ppm along with the increase in intensity of the singularity at 505 ppm. The apparent "mirror image" nature of the simulated line shape, in comparison with the experimental, can only be explained as being due to the presence of an impurity in the sample, causing a distortion of the experimental spectrum.

Another example of a mixed tetrahedral/octahedral site compound, similar to $[Mo_2O_7]^{2-}$, is $[Mo_8O_{26}]^{4-}$. The structure consists of six octahedra and two tetrahedra condensed into a cagelike structure.[62] The static powder line shape (Figure 7a) consists of two components (Figure 7d): a narrow line ($W_{1/2} \sim$ 4.5 kHz, Q_{cc} = 0.34 MHz, η_Q = 0.0, σ_{11} = −35 ppm, σ_{22} = −35 ppm, σ_{33} = 10 ppm), corresponding to the two tetrahedral molybdenum sites, superimposed on a broader line ($W_{1/2} \sim$ 25 kHz, Q_{cc} = 6.12 MHz, η_Q = 0.53), corresponding to the six octahedral sites for molybdenum. The distinction between the two line shapes is accentuated by the 3.3-kHz MAS spectrum (Figure 7b), in which the tetrahedral resonance narrows to a greater extent than does the octahedral resonance. This, of course, is to be expected as the tetrahedral line shape is dominated by a CSA/dipolar interaction, which is averaged by the MAS experiment. The octahedral site, however, possesses a larger Q_{cc}, which dominates the line shape. The MAS experiment does not narrow this octahedral line shape effectively.[63]

The static powder spectrum of $H_3PMo_{12}O_{40}$ (Figure 8a) clearly demonstrates the size to which a Q_{cc} can grow in an octahedral environment. The large Q_{cc} of ~6.5 MHz is the result of having six different Mo–O distances (1.69–2.42 Å) in each of the 12 octahedra of the complex.[64] The narrowing of the line shape, by MAS, for the tetrahedral molybdenum in $Al_2(MoO_4)_3$ (Figure 8c,b) is not as dramatic as expected from observation of other tetrahedral species. In the static spectrum, a small peak appears at −71 ppm, next to the $Al_2(MoO_4)_3$ peak at −322 ppm. This small peak may be due to unreacted MoO_3 present in the sample. The peak at −322 ppm narrows from 3.04 to 1.77 kHz on MAS at 3.7 kHz, which is not as large a narrowing as was observed for the other tetrahedral model compounds. The crystal structure of $Al_2(MoO_4)_3$ is isostructural with that of $Sc_2(WO_4)_3$, which has W atoms in distorted tetrahedral sites.[65] The chemical shift of $Al_2(MoO_4)_3$ will become quite important in later discussions as it seems that $Al_2(MoO_4)_3$ is present in the catalyst samples that we have investigated.

The fact that the polyoxomolybdates species all fall in a small chemical shift range means that it will be difficult to identify individual species on the catalyst surface. However, the line widths and the effect of MAS on the line widths may allow one to be able to distinguish between octahedral (low symmetry), and tetrahedral (relatively high symmetry) sites on the surface. Although it must be noted that octahedral environments can, in some cases, possess high symmetry and thus possess only a small value of Q_{cc}.

Investigation of Catalyst Samples. Before we begin our discussion of the catalyst samples themselves we will first address the question of the loading of molybdenum on the surface. This

(61) Nagano, O.; Sasaki, Y. *Acta Crystallogr.* **1979**, *B35*, 2387.
(62) Vivier, H.; Bernard, J.; Djomna, H. *Rev. Chim. Miner.* **1977**, *14*, 584.
(63) Ganapathy, S.; Schramm, S.; Oldfield, E. *J. Chem. Phys.* **1982**, *77*, 4360.
(64) d'Amour, H.; Allmann, R. *Z. Kristallogr.* **1976**, *143*, 1.
(65) Abrahams, S. C.; Bernstein, J. L. *J. Chem. Phys.* **1966**, *45*, 2745.

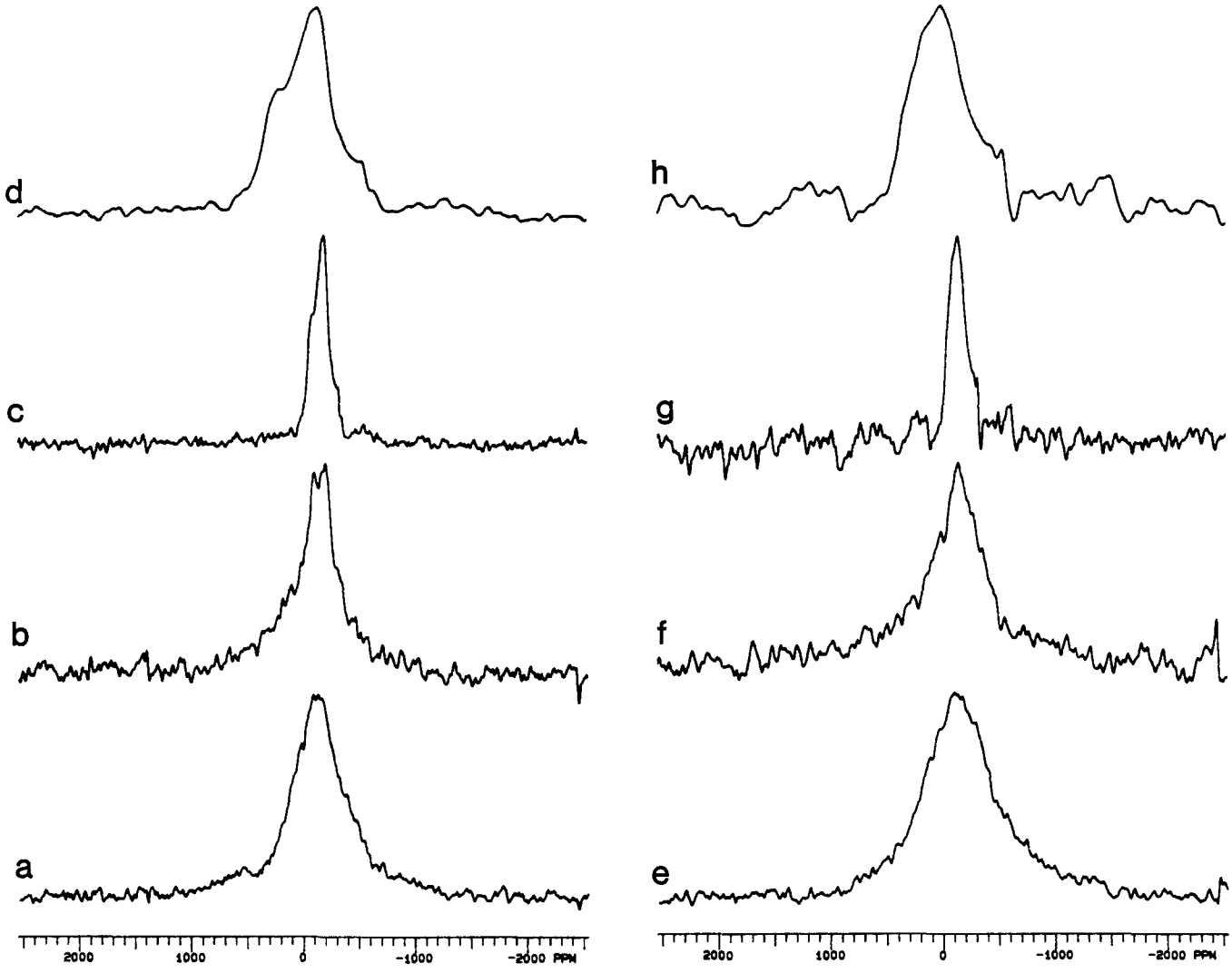

Figure 9. Static powder and MAS spectra of the central $\pm^1/_2$ transition of calcined and uncalcined 24% wt/wt MoO_x–Al_2O_3 catalysts. (a) Static powder spectrum of the uncalcined catalyst, 154 000 transients. (b) The 3.0-kHz MAS spectrum of the uncalcined catalyst, 96000 transients. (c) The 9.62-kHz MAS spectrum of uncalcined catalyst, 245 000 transients. (d) The expansion of c. (e) Static powder spectrum of the calcined catalyst, 330 000 transients. (f) The 4.3-kHz MAS spectrum of the calcined catalyst, 96 000 transients. (g) The 8.45-kHz MAS spectrum of the calcined catalyst, 188 000 transients. (h) The expansion of g. The relaxation delay was 0.05 s and the applied line broadening was 500 Hz in the case of the uncalcined catalyst spectra and 750 Hz in the case of the calcined catalyst spectra.

was determined by a Beer's law plot, from our NMR spectra, of calcined and uncalcined catalyst samples at loadings of 3%, 6%, 8%, and 12%. We plotted the signal-to-noise ratios of the calcined and uncalcined catalyst spectra against the loading (% wt/wt). The plots revealed that, within experimental error, Beer's law is fulfilled. The actual amount placed on the surface, however, may or may not be effected by a scaling factor.

The static powder line shapes of the various loading uncalcined and calcined catalysts (results not shown) look very similar apart from an increase in line width. From Table II it can be seen that there is some variation in the line width of the uncalcined samples from 13.3 to 17.04 kHz. It should be noted that in every case the line width increased on calcination by a considerable amount, the magnitude of the increase varying from 3.11 (for the 24% Mo catalyst) to 7.02 kHz (for the 16% Mo catalyst). The exception being the 12% Mo catalyst prepared at pH 9.0 whose line width increases by only 0.50 kHz. This broadening could well be due to a further lowering of the symmetry of the oxomolybdo surface species on formation of an oxygen-bridged polymeric species by condensation of the molybdenum species with each other and with the surface hydroxyls to form a polymeric species with a larger Q_{cc} (owing to the greater degree of distortion usually present in octahedral molybdenum sites in polymeric polyoxomolybdates[55]).

Effect of pH during the Impregnation Procedure. The preliminary results on the effect of pH of the impregnation solution on the species adsorbed on the alumina surface were obtained with on a catalyst whose loading was 8% wt/wt of heptamolybdate, in a pH-adjusted impregnation solution (results not shown), the pH adjustment being to pH 5.2 and 8.2 in this case. The predominant molybdenum oxoanions present *in solution* at the various pH can be represented as

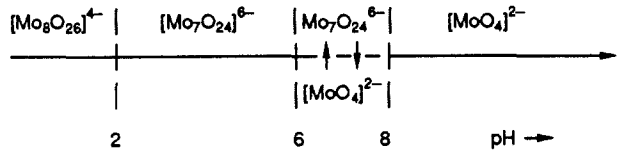

This means that in our impregnation solutions of pH 5.2 and 8.2 we have predominantly $[Mo_7O_{24}]^{6-}$ and $[MoO_4]^{2-}$ present, respectively. The isoelectric point (IEP) of the alumina, at pH ~8, is such that at a pH of 5.2 the hydroxyl groups of the alumina are protonated and there is a mechanism of adsorption possible due to electrostatic attraction between the oxomolybdenum anions and the protonated surface. Wang and Hall[14] suggested that this leads to the heptamolybdate adsorbing to the surface intact, and that these surface clusters remain intact. During calcination they are bound to the surface by reaction with the surface hydroxyls leading to polymeric clusters of octahedral/tetrahedral polyoxomolybdenum species. The situation is quite different when the impregnation solution is at a higher pH than the IEP of the alumina. The surface hydroxyls are deprotonated, leading to a

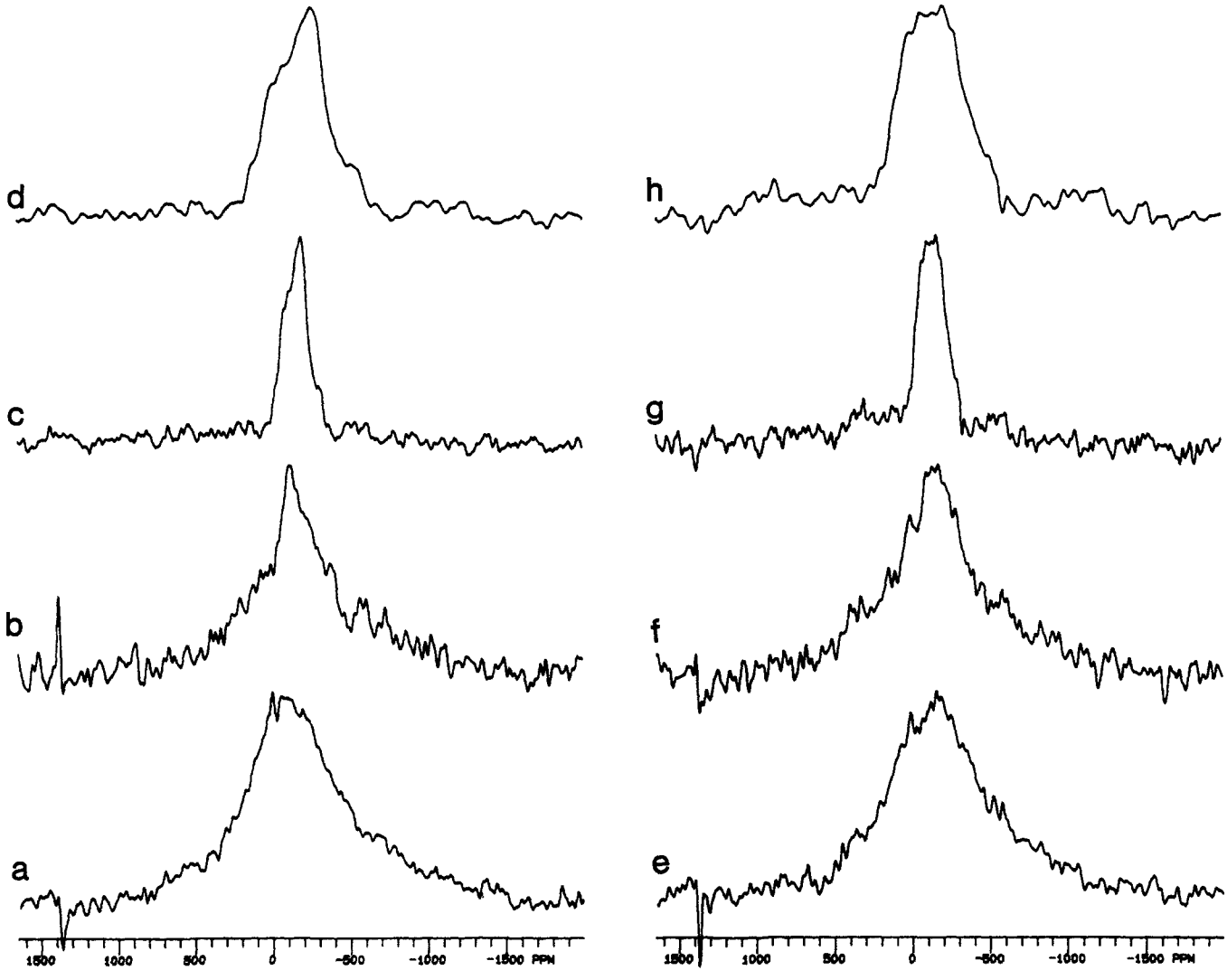

Figure 10. Static powder and MAS spectra of the central $\pm^1/_2$ transition of uncalcined and calcined 12% wt/wt MoO_x–Al_2O_3 catalysts prepared at pH 9.0. In all cases except where stated, the relaxation delay was 0.05 s and the applied line broadening was 500 Hz. (a) Static powder spectrum, uncalcined, 346 000 transients. (b) The 4.3-kHz MAS spectrum, uncalcined, 96 000 transients. (c) The 9.60-kHz MAS spectrum, 404 000 transients. (d) Expansion of c. (e) Static powder spectrum, calcined, 150 000 transients. (f) The 4.2-kHz MAS spectrum, 150 000 transients. (g) The 10.35-kHz MAS spectrum, 460 000 transients. (h) Expansion of g.

net negative charge at the alumina surface that prevents adsorption of the tetrahedral $[MoO_4]^{2-}$ present in the solution. As the catalyst dries, the molybdate is thought to be precipitated onto the surface. (Whether this precipitated salt is deposited as a disordered or ordered phase that interacts with the alumina surface or as a bulk salt species closely associated with a counterion will be discussed later.) During calcination these precipitates are oxidized to MoO_3 crystallites. When examined closely, the spectra obtained for the two different pH cases (pH 5.2 and 8.2) are both virtually identical with the spectra obtained at other loadings with an impregnation pH of 5.2. This is surprising, as one might expect the catalysts prepared at a pH of 8.2 to give a narrower resonance as one would expect the uncalcined catalyst to have a saltlike $[MoO_4]^{2-}$ phase present. However, the description of the surface chemistry occurring at any one pH is not as simple as was previously described.

It has been argued that at low pH (pH <7) the surface gains a net positive charge due to the protonation of the surface hydroxyls. It such cases there will always be a net shift in the pH of the impregnation solution back toward the IEP of the alumina, which in turn will effect the solution-state equilibrium reaction

$$7MoO_4^{2-} + 8H^+ \rightleftharpoons Mo_7O_{24}^{6-} + 4H_2O \qquad (4)$$

How far the equilibrium will shift depends upon the relative concentrations of the $[H^+]$ in solution and the surface hydroxyls. It is possible therefore to have both $[Mo_7O_{24}]^{6-}$ and $[MoO_4]^{2-}$ in the impregnation solution. If one is in a regime in which [surface–OH] > $[H^+]$, one will have the possibility of having coadsorption of both tetrahedral and octahedral molybdates onto the surface, In the case of an impregnation at a pH higher than the IEP of the alumina (>pH 8), one is in a situation where the surface hydroxyls are deprotonated by the solution hydroxyls, generating a net negative charge on the surface. However, this again causes a shift in the solution pH back toward the IEP of the alumina, which again causes a shift in the equilibrium (eq 4). Thus, octahedral molybdate can be present in this situation. Another important point to note is that as the solution hydroxyls deprotonate the surface hydroxyls it is likely that the $[NH_4]^+$ cations will become associated with the negatively charged sites, thus preventing a buildup of negative charge. This fact, combined with the importance of the relative concentrations of the surface and solution hydroxyl ions (in the situation when [surface–OH] > $[OH^-]$, not all the surface hydroxyls will be deprotonated), means that there will still be sites available for ion exchange and the net negative charge will not always be strong enough to prevent such adsorption. Thus, the overall picture of the species that can be deposited on the surface may be similar regardless of the pH of the impregnation solution.

Exploitation of the MAS Experiment as a Spectral Editor. Owing to the similarity of the static powder spectra, we cannot extract any information that can help us understand the multicomponent surface structure of the catalysts. We can, however, address this problem by examining how the line shapes of the

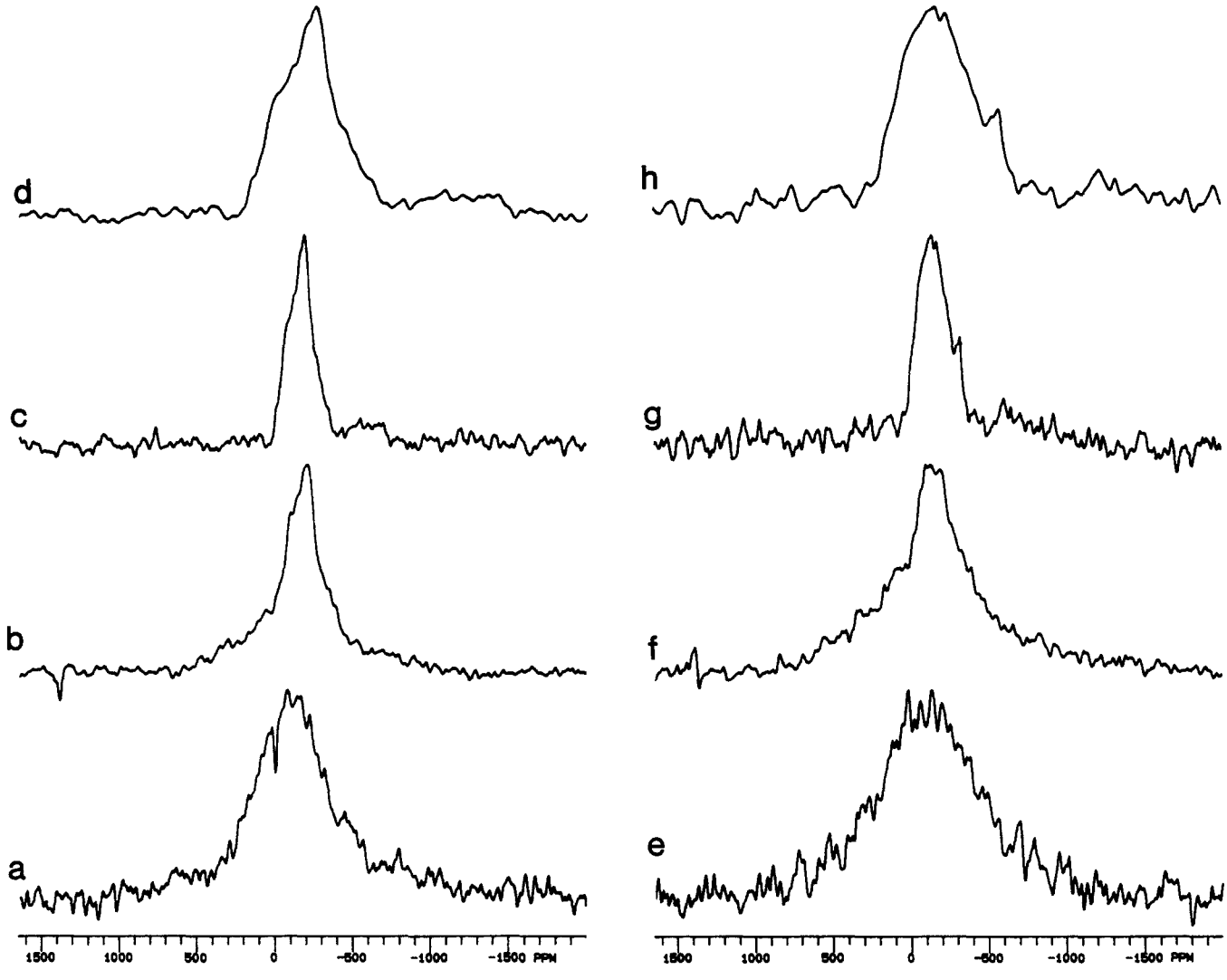

Figure 11. Static powder and MAS spectra of the central $\pm^1/_2$ transition of uncalcined and calcined 12% wt/wt MoO_x–Al_2O_3 catalysts prepared at pH 5.2. In all cases except where stated, the relaxation delay was 0.05 s and the applied line broadening was 500 Hz. (a) Static powder spectrum, uncalcined, 300 000 transients. (b) The 4.4-kHz MAS spectrum, uncalcined, 386 000 transients. (c) The 10.03-kHz MAS spectrum, 360 000 transients. (d) Expansion of c. (e) Static powder spectrum, calcined, 267 000 transients. (f) The 4.2-kHz MAS spectrum, 387 000 transients. (g) The 11.23-kHz MAS spectrum, 364 000 transients. (h) Expansion of g.

catalyst change when acquired by an MAS experiment. From the behavior of the model compounds, one might expect, in a catalyst containing multiple molybdenum species, to observe a differential narrowing of the component line shapes, dependent on the spinning speed and the Q_{cc} of the species present on the surface. Accompanied with this narrowing may be the possibility of distinguishing between the species on a chemical shift basis. With this in mind we have investigated the MAS line-shape behavior of several catalysts—namely, a 24% loading catalyst prepared at pH 5.2 and a range of 12% loading catalysts prepared at pH 2, 5.2, and 9.

Figure 9a–h shows the effect of magic angle spinning on the line shapes of calcined and uncalcined 24% wt/wt MoO_x–Al_2O_3 catalysts prepared at pH 5.2. Parts a–d of Figure 9 show the comparison of the static powder, 3.0- and 9.6-kHz MAS line shapes of the uncalcined catalyst, while parts e–h of Figure 9 show the comparison of the static powder, 4.3- and 8.5-kHz MAS line shapes of the calcined catalyst. Of immediate interest is the appearance of the feature at ~530 ppm in the static powder spectrum of the uncalcined sample, perhaps indicative of the precipitation of intact $[Mo_7O_{24}]^{6-}$ salt onto the surface (see the corresponding singularity in static powder spectrum of heptamolybdate in Figure 5a). As can be seen from these line shapes, there is a considerable narrowing of the line shape under MAS conditions. The slow spinning speed MAS spectra for the calcined and especially for the uncalcined catalysts seem to indicate that there may be more than one component to the line shape. The 3.0-kHz MAS spectrum of the uncalcined sample (Figure 9b) shows considerable narrowing in the upper portion of the spectrum and the resolution of two singularities at −109 and −204 ppm, while the lower portion remains relatively broad. At 9.62-kHz MAS the broader component has been effectively narrowed and there are three singularities in the line shape (Figure 9c,d), at −83, −193, and −294 ppm. However, one must be careful when attempting to make an assignment of these singularities, as the MAS of second-order quadrupole line shapes leads to line shapes with multiple singularities, the positions of which vary with spinning speed. This negates the possibility of assigning each singularity to a different species. However, as we will see later, it can be justified to treat the line of the uncalcined catalysts as multiple-component line shapes containing two to three components.

The calcined 24% Mo–Al_2O_3 sample, other than being broader, appears to be similar to the spectra obtained for the uncalcined samples. The static powder spectrum is 3.1 kHz broader than the uncalcined and shows no significant chemical shift differences. The MAS spectra, however, show a chemical shift difference from the uncalcined catalyst, with the 8.5-kHz MAS spectrum (Figure 9g,h) showing features at −152 and −295 ppm. The line shape is broader than the high-speed MAS spectrum line shape of the uncalcined catalyst, which may be due to the formation of a polymeric species similar to MoO_3 with a large quadrupole interaction.

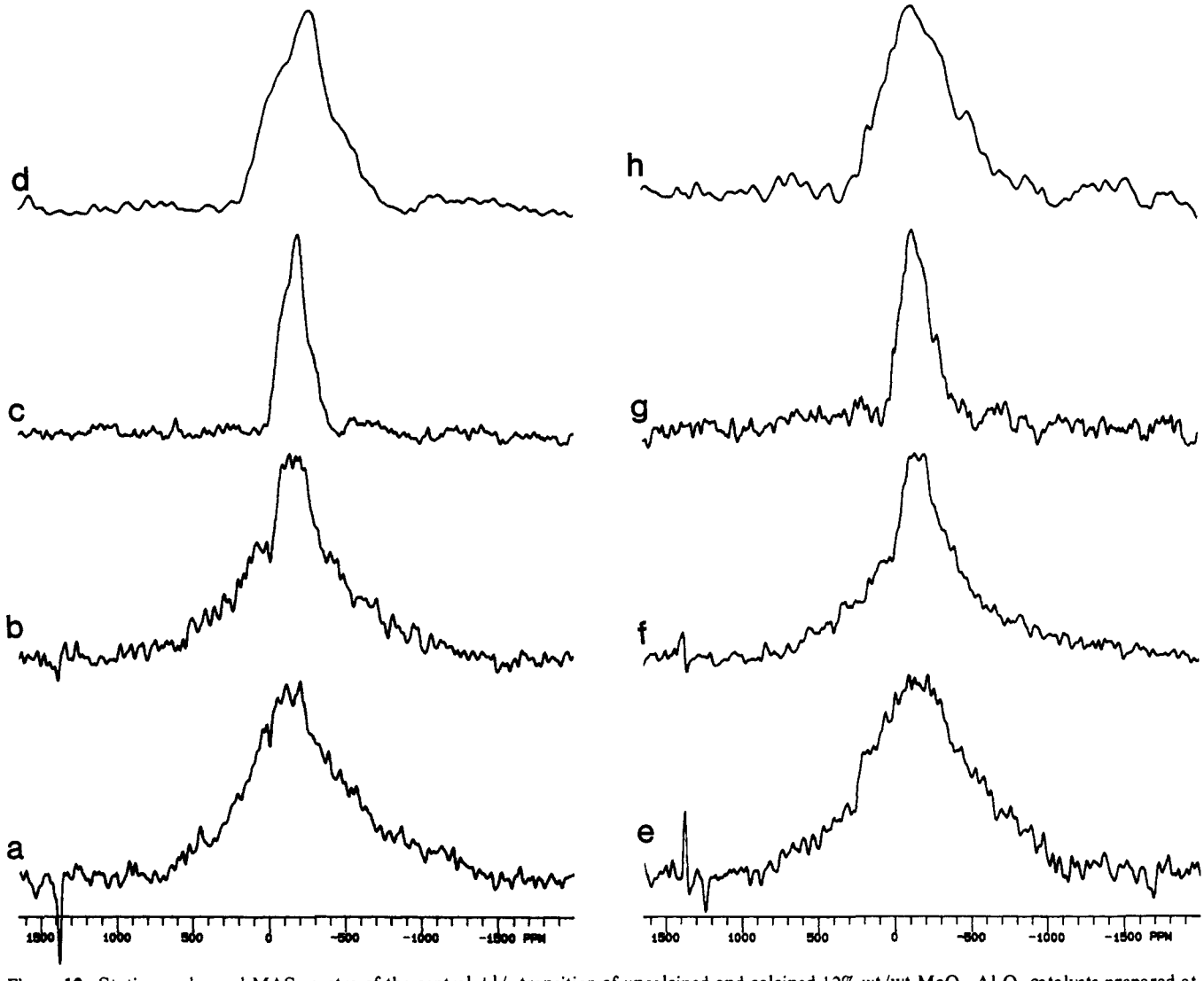

Figure 12. Static powder and MAS spectra of the central $\pm^1/_2$ transition of uncalcined and calcined 12% wt/wt MoO_x–Al_2O_3 catalysts prepared at pH 2.0. In all cases except where stated, the relaxation delay was 0.05 s and the applied line broadening was 500 Hz. (a) Static powder spectrum, uncalcined, 250 000 transients. (b) The 4.5-kHz MAS spectrum, uncalcined, 250 000 transients. (c) The 11.52-kHz MAS spectrum, 530 000 transients. (d) Expansion of c. (e) Static powder spectrum, calcined, 150 000 transients. (f) The 4.5-kHz MAS spectrum, 140 000 transients. (g) The 12.2-kHz MAS spectrum, 468 000 transients. (h) Expansion of g.

In order to confirm this narrowing of the line shapes and the resolution of the three singularities, the experiment was repeated for three 12% MoO_x–Al_2O_3 catalysts prepared at different pH. Another reason for wanting to study catalysts prepared at different pH was that a particular species can be made to be predominantly present in the impregnation solution. This might enable an easier interpretation of any differences in the line shapes that might arise. Figure 10a–h shows the effect of MAS on the line shape obtained for a 12% MoO_x–Al_2O_3 catalyst prepared at pH 9.0, while Figure 11a–h and Figure 12a–h show the effect of MAS on 12% Mo–Al_2O_3 catalysts prepared at pH 5.2 and 2.0, respectively.

First, we will discuss the results obtained for the 12% Mo uncalcined samples (Figures 10a–d, 11a–d, and 12a–d). A systematic study of the singularity positions of the MAS spectra obtained at different pH yields some very interesting conclusions, which will be discussed later. The 4.3-kHz MAS spectrum for the pH 9 catalyst (Figure 10b), with predominantly $[MoO_4]^{2-}$ present in the impregnation solution, yields an intense singularity at −118 ppm, a shoulder at ∼−200 ppm, and a broader underlying resonance. Upon high-speed spinning, at 9.6 kHz (Figure 10c,d), the line shape is effectively narrowed, with the most intense singularity appearing at −183 ppm and shoulders appearing at −83 and −295 ppm.

Considering the catalyst prepared at pH 5.2 with predominantly heptamolybdate in the impregnation solution, the 4.4-kHz MAS spectrum (Figure 11b) shows a singularity at −209 ppm (91 ppm shifted from the feature seen for the sample prepared at pH 9 observed at the same spinning speed), along with a well-defined shoulder at ∼−110 ppm. The broad underlying resonance is reduced in comparison with the pH 9 case. The high-speed MAS spectrum (Figure 11c,d) again shows an effectively narrowed line shape very similar to that seen in the pH 9 case, with an intense singularity at −193 ppm and shoulders appearing at −100 and −299 ppm.

Finally, the sample prepared at pH 2, which has $[Mo_8O_{26}]^{4-}$ present in the impregnation solution, has both octahedral and tetrahedral sites present in the cluster. The 4.5-kHz MAS spectrum (Figure 12b) does not narrow to the same extent as the catalyst samples prepared at other pH. However, the line shape has singularities at both −118 and −196 ppm, indicating that the line shape may be a superposition of the low spinning speed line shapes of the previous two pH values. The high-speed MAS spectrum (Figure 12c,d) is virtually identical with the high-speed MAS spectrum obtained for the pH 9 and pH 5.2 catalysts.

Interpretation of the Catalyst Line Shapes. The problem that we have encountered in the interpretation of the static and high spinning speed MAS results is that the line shapes look almost identical apart from a few minor differences such as the intensities of certain shoulders. We do, however, have a way of extracting information on the species present in these line shapes. From the model compound studies,[55] we have found that one can edit the spectra by using the differential narrowing that different species

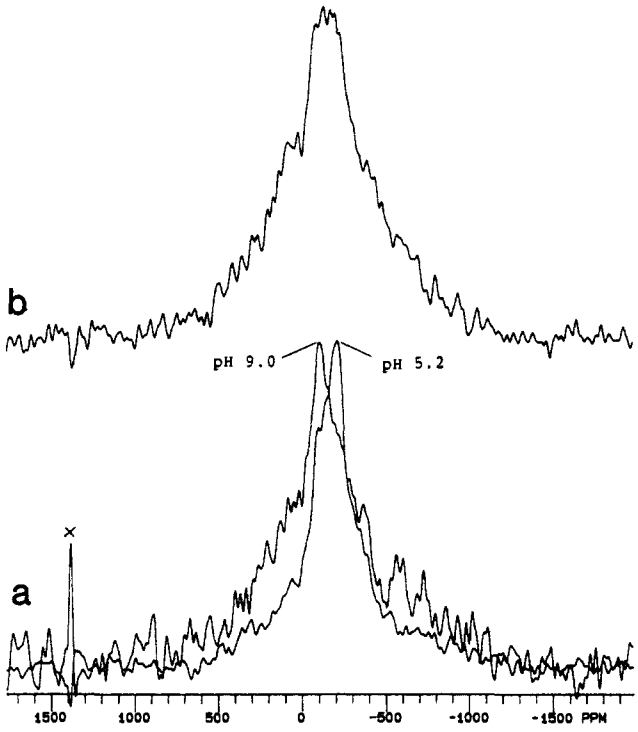

Figure 13. The slow spinning (~4.4-kHz) MAS spectra of 12% Mo–Al_2O_3 catalysts prepared at different pH. (a) The superposition of (i) the 4.3-kHz MAS spectrum of a catalyst prepared at pH 9.0 and (ii) the 4.4-kHz MAS spectrum of a catalyst prepared at pH 5.2. (b) The 4.5-kHz MAS spectrum of a catalyst prepared at pH 2.0.

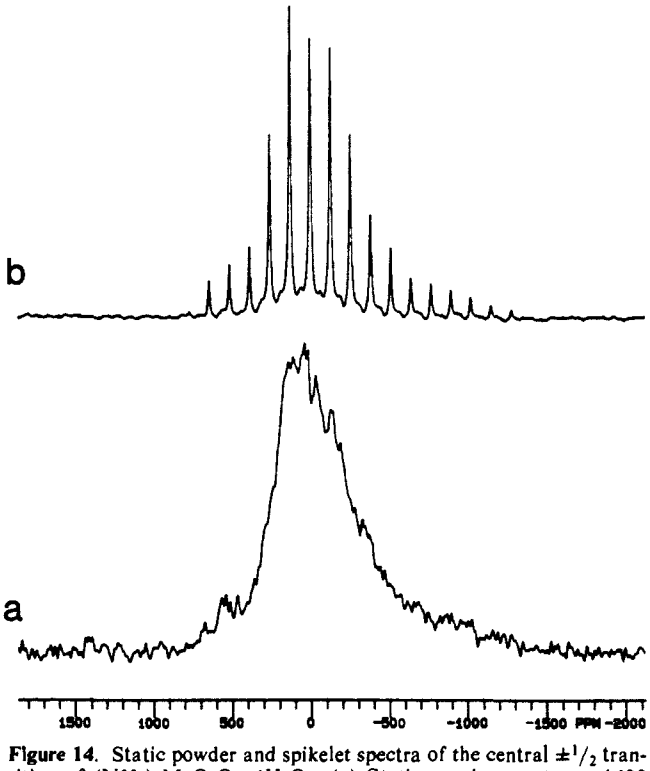

Figure 14. Static powder and spikelet spectra of the central $\pm^1/_2$ transition of $(NH_4)_6MoO_7O_{24}{\cdot}4H_2O$. (a) Static powder spectrum, 1600 transients, d1 = 2 s, LB = 250 Hz. (b) Spikelet solid echo spectrum, 20480 transients, d1 = 1 s, LB = 250 Hz.

undergo depending on the value of Q_{cc}. It has been found that species with small quadrupole interactions are effectively narrowed by MAS experiments performed at low spinning speeds (2–5 kHz) while the species with larger quadrupole require higher spinning speeds (7–12 kHz) to be effectively narrowed. At the lower spinning speed, the MAS results indicate that the high-speed MAS line shapes are made up of multiple components rather than an

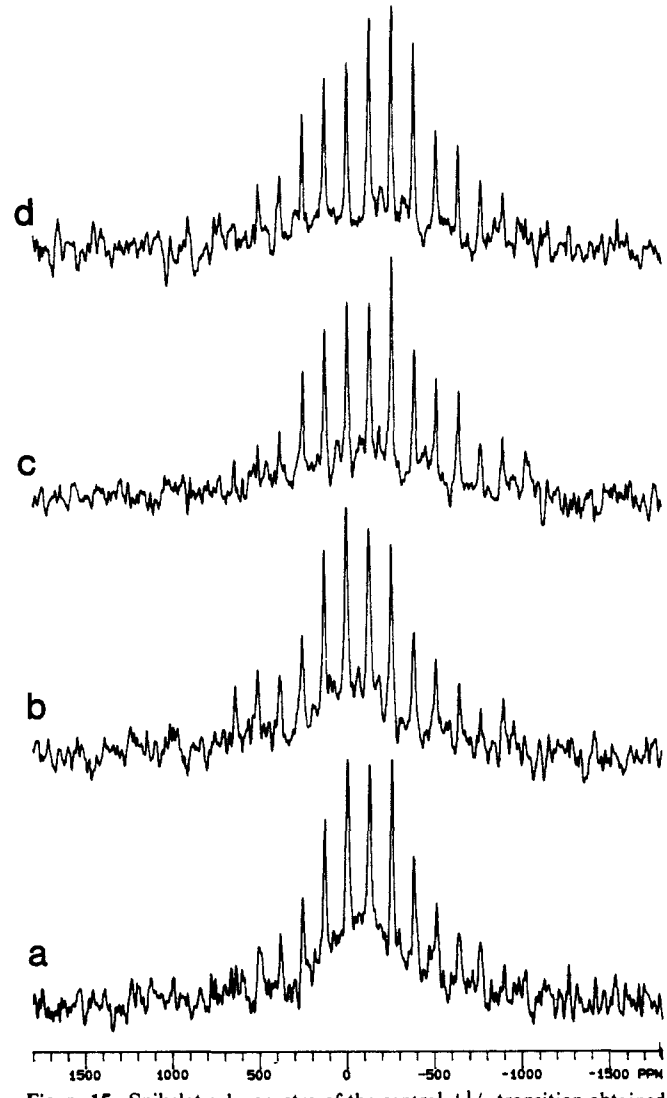

Figure 15. Spikelet echo spectra of the central $\pm^1/_2$ transition obtained for uncalcined and calcined MoO_x–Al_2O_3 catalysts with 16% and 24% loadings. In each case the number of transients taken was 100×10^3, the applied line broadening was 300 Hz, and the relaxation delay was 0.075 s. (a) 16% uncalcined, (b) 24% uncalcined, (c) 16% calcined, and (d) 24% calcined.

averaged, single-component, second-order quadrupole line shape. In the low spinning speed cases (Figures 10b, 11b, and 12b), the spinning speed is basically the same yet the line shapes are different. (If the line shapes were simply those of a single species whose line shape was not adequately averaged by the MAS technique, one would expect the line shapes to be the same at the same spinning speed.) This indicates that different molybdate species are predominant on the surface, depending on the pH of the impregnation solution. One thing that is clear, from the model compound studies, is that the line shapes observed for both static and MAS catalyst samples do not resemble the line shapes one would expect if the surface species were intact precipitates of $(NH_4)_6Mo_7O_{24}$, MoO_3, or $(NH_4)_2MoO_4$. Also, the resonances do not appear in the expected chemical shift range. Due to this fact we feel that we are observing solely adsorbed molybdate species.

To clarify the differences in the slow-spinning MAS line shapes, we have shown Figure 13. In Figure 13a we have the superposition of the 12% Mo–Al_2O_3, slow-spinning MAS line shapes of catalysts prepared at pH 9.0 and 5.2. The difference in the peak maxima is 90 ppm. Based on the suposition that the adsorbed tetrahedral and octahedral species will be chemically shifted from each other and produce different, partially averaged slow MAS line shapes, we can offer an explanation for this observation. At pH 9, the predominant species in solution is $[MoO_4]^{2-}$, and the chemistry

involved in the impregnation procedure at this pH indicates that the molybdenum might be present on the surface predominantly as adsorbed $[MoO_4]^{2-}$. This species should have a small quadrupole interaction, which will be effectively narrowed at low spinning speeds in MAS experiments. Indeed, in the low spinning speed MAS experiment (Figure 10b) we observe an intense singularity at −118 ppm. However, this feature is chemically shifted by over 100 ppm to higher shielding compared to the tetrahedral model molybdate species. It should also be noted that there is a weak shoulder at ~−200 ppm. In previous work[28] involving the adsorption of Rb^+ to γ-alumina, Cheng and Ellis demonstrated that, at submonolayer coverages, one observes the deposition of bulk salt ("surface salt") onto the surface as well as a surface-interactive salt species ("surface species"). The surface species was found to consist of two different species, which could be placed into two categories—an ordered phase and a disordered phase. The ordered phase was found to be static, surface-bound Rb^+ while the disordered phase was a dynamically active species that was interacting with the surface. The chemical shift differences observed for the bulk salt and the surface salt differed by ~120 ppm due to higher shielding. Thus, it has been demonstrated that interaction with an alumina surface can cause a considerable shift to higher shielding, independent of whether the surface species is ordered or disordered. Thus, we hypothesize that the narrowed line-shape component that we are observing is a tetrahedral molybdate surface species, which is interacting with the surface but retains a relatively small Q_{cc} value. The significance of the shoulder at ~−200 ppm will be discussed later. The broad underlying component of the line shape may be due to several factors, including, incompletely averaged chemical-shielding interactions, possible dynamically active species, and other, as yet undefined, surface species. The presence of the adsorbed surface species at this pH demonstrates that the notion that only precipitation of bulk $[MoO_4]^{2-}$ salt occurs upon drying of the sample is erroneous. A situation similar to the one described previously, with very little negative charge buildup at the surface, must indeed be occurring at this pH in order for adsorption to have taken place, i.e., equilibrium 4. It is apparent that if precipitation of surface salt does occur, the precipitated salt interacts strongly with the surface.

The pH 5.2 catalyst low spinning speed spectrum shows an intense feature at −209 ppm with a shoulder at −110 ppm. The obvious differences between this line shape and the line shape observed for the pH 9 catalyst obtained at the same spinning speed indicates that different species predominate in the two catalysts. The predominant species in the impregnation solution, at this pH, is $[Mo_7O_{24}]^{6-}$. One would expect then that octahedral molybdate would be the predominant species present on the alumina surfaces. (Although it should be noted that the adsorption mechanism, at this pH, does facilitate the adsorption of $[MoO_4]^{2-}$ by the dissociation of the heptamolybdate clusters brought about by the buffer effect of the alumina hydroxyls.)[14,26] Thus, a possible explanation for the narrowed features is that the shoulder at −110 ppm is due to the presence of a surface-adsorbed, tetrahedral molybdate species [formed because of the shift in the equilibrium (eq 4) caused by the presence of excess surface hydroxyls], while the feature at −209 ppm is due to adsorbed octahedral molybdate. In order for the adsorbed octahedral species to narrow as it does it must possess a relatively small quadrupole interaction, and thus it is likely that these species are singly adsorbed octahedral units or small heptamolybdate fragments. Again, the fact that the resonance is shifted to higher shielding compared to the model octahedral compounds supports the hypothesis that this species is interacting with the surface. (Thus, it seems likely that in the slow-spinning MAS spectrum of the pH 9 catalyst, the weak shoulder present at ~−200 ppm indicates the presence of a small amount of adsorbed octahedral molybdate.) Again, a broad underlying component is observed, which is caused by incompletely averaged shielding interactions of the two types of adsorbed molybdate.

The high-speed MAS spectrum is virtually identical with that obtained for the pH 9 catalyst except for the relative intensities of the shoulders at ~−90 ppm. This is to be expected as the same species are present on the surface. The only difference is in the relative concentrations of the two components at the different pH.

In Figure 13b we have the low spinning speed MAS spectrum of the catalyst prepared at pH 2, which has a mixed tetrahedral/octahedral species as the predominant impregnation species. As one might expect, according to our hypothesis, the line shape yields the presence of both tetrahedral and octahedral disordered molybdenum surface species in more closely equal relative amounts. However, the broad underlying resonance is more intense than in the previous two cases, perhaps indicating the presence of a larger chemical shielding interaction. The high-speed MAS results, again, are almost identical with those obtained previously. At this pH, the overall net positive charge of the alumina surface should facilitate better adsorption of the molybdate anions.

Thus, we can say that the slow spinning speed MAS spectra consist of two components—surface-adsorbed octahedral and tetrahedral molybdate. The differences in the line shapes are caused by the differences in concentration of the two types of surface species at different pH. However, the fact that the same two types of species are present on the surface in all cases yields high spinning speed MAS line shapes that appear very similar except for the relative intensities of certain shoulders.

Finally, we must mention the shoulder that appears at around −290 to −300 ppm in all the high-speed MAS spectra. There are two possibilities as to the identity of this singularity. First, it may be a shoulder of one of the MAS averaged, second-order quadrupole line shapes, the center of which resonates to lower shielding. Second, this singularity position corresponds, almost exactly, to the MAS peak position of $Al_2(MoO_4)_3$ (see Figure 8c). Thus, it may be that $Al_2(MoO_4)_3$ is present in the uncalcined samples.

The calcined samples on the other hand (Figures 10e–h, 11e–h, and 12e–h) are all very similar, indicating that although different proportions of octahedral and tetrahedral molybdenum species are formed on the surface during impregnation, the calcination yields a similar polymeric species regardless of the impregnation procedure. The high-speed MAS spectra (Figures 10g,h, 11g,h, and 12g,h) show a peak at ~−140 to −160 ppm, indicative of the formation of a new polymeric species. In the case of the calcined catalysts, the shoulder at ~300 ppm is much more pronounced and could be considered as a peak rather than a shoulder. This is perhaps indicative of the presence of a higher concentration of $Al_2(MoO_4)_3$.

In an effort to ascertain if the MAS spectra were simply the product of removing dipolar broadening (i.e., if the CSA was small), several of the samples were run with proton decoupling. The static spectrum was taken of the heptamolybdate salt and it showed a line narrowing of 1.17 kHz, but the overall features of the line shape remained the same. The static powder spectra of the uncalcined samples also showed a small reduction in line width upon ^1H decoupling. The reductions in line width of the uncalcined catalysts were 0.74 kHz for the 12% Mo sample and 1.72 kHz for the 24% Mo sample. The catalyst line shape also retained its overall characteristics.

Spikelet Echo Experiments. One more experiment is available to us if we wish to resolve whether there are dynamically active, surface-interactive molybdate or MoO_3 precipitates on the surface. If there are dynamically active, disordered surface species on the surface one would expect to find different mobility for these species compared to the ordered, adsorbed surface species. These differences in mobility should be reflected by a variation in their respective spin–spin relaxation times, T_2. One way to illustrate the existence of species of differing dynamic character is to perform the spin–echo spikelet experiment.[28,29] As was explained previously, this involves a solid–echo sequence followed by a train of $(\pi)_s$ pulses, which generates a transverse magnetization consisting of a series of refocused solid echoes. Fourier transformation of this signal leads to a spectrum consisting of narrow resonances, which appear at positions modulo $(2\tau)^{-1}$ apart. The widths of these narrow "spikelets" denote only the homogeneous contributions to the powder line shape. The problems encountered in running these spectra, such as FID truncation, digitization, removal of DC offset,

chemical shift scaling, etc., are discussed fully in the work of Cheng and Ellis.[28]

Figure 14a,b shows the effect of the spikelet experiment on the line shape of $(NH_4)_6Mo_7O_{24}\cdot 4H_2O$. The static powder spectrum of the central $\pm^1/_2$ transition of the heptamer species is displayed in Figure 14a while the spikelet spectrum is shown in Figure 14b. It should be noted that the spikes (or lines) that result from this experiment do not extend far beyond the static powder line shape. The line widths of the spikes vary from 218 to 300 Hz and appear at intervals of 3.33. kHz (128 ppm), about the spikelet at 0 ppm, which corresponds to the expected value of $(2\tau)^{-1}$ as the value of τ was 150 μs in all of the spikelet experiments that were performed. It should be noted that there are several other impurity species in our sample of heptamolybdate, which appear as chemically shifted spikelets that give the appearance of a broader resonance and less intense spikelets underlying the heptamolybdate spikelets.

Owing to the similarity of the isotropic chemical shifts of the $[MoO_4]^{2-}$ and $[Mo_7O_{24}]^{6-}$ species, they will not yield resolved spikelets. This is due to the scaling of the chemical shift that occurs due to the short cycle time of the echo train. The chemical shift of the species will be preserved if the π pulse repetition rate frequency is small in comparison with the chemical shift separation in hertz. In this case, however, the pulse repetition rate is on the order of 3.30 kHz while the maximum chemical separation of the species we are concerned with is around 34–0 ppm (0.89–0 kHz) for $[Mo_7O_{24}]^{6-}$ and $[MoO_4]^{2-}$, 100 ppm (2.6 kHz) for MoO_3, and 300 ppm (7.82 kHz) for $Al_2(MoO_4)_3$. One should definitely observe chemically shifted spikelets if $Al_2(MoO_4)_3$ were present. These chemically shifted spikelets, if they exist, would appear as a pattern of lines that did not have a modulo $(2\tau)^{-1}$ spacing relative to the other species.[28] If we have species present on the surface with considerably different T_2 values, this will lead to a spectrum of lines with different widths dependent on the $_{T2}$ of a given species. This T_2 dependence can support the presence of dynamically active surface species as T_2 is motion modulated.

Depicted in Figure 15a–d are selected spikelet spectra of uncalcined and calcined catalysts prepared with an impregnation solution at pH 5.2 at loadings of 16% Mo and 24% Mo. The line widths of the spikelet resonances vary from 401 to 817 Hz and as expected occur at ~3.30-kHz separation. The striking feature present in Figure 15a and b, which is absent in Figure 14b, is the broad (~7 kHz) resonance. Since this experiment distinguishes species based upon differences in T_2, it is immediately clear that there are species present with very different T_2 values. Hence, the surface is dynamically inhomogeneous. That is, there appear to be species that are immobilized on the surface (long T_2) and species with high mobility (short T_2's).

The spikelet spectrum obtained for the uncalcined 12% Mo catalyst prepared at pH 5.2 (spectrum not shown) does not reveal the presence of a broad underlying resonance and thus indicates the absence of any dynamic surface species. This is in agreement with the MAS results, which only revealed the presence of adsorbed surface species which one would not expect to be dynamically active.

The broad resonance disappears to a large extent upon calcination, leaving only a small trace of itself in the spikelet spectra of the higher loading (16% and 24% wt/wt) calcined catalysts (Figure 15c,d). In line with the MAS data, discussed previously, we propose that the dynamic species may be disordered tetrahedral/octahedral surface molybdate species[28] or small amounts of precipitated surface salt. These species are either adsorbed to the surface or polymerized with existing molybdenum surface species during calcination. The fact that there is a dynamic species is also demonstrated by the increase in the signal-to-noise ratio observed for the spikelet lines that occurs upon calcination. This indicates that a larger proportion of the molybdenum species are static after calcination.

In all of the spectra (calcined and uncalcined) there appear to be chemically shifted spikelets of much lower intensity than the ones previously discussed. These spikelets could be due to the presence of $Al_2(MoO_4)_3$, which one would expect to be chemically shifted on the basis of the pulse repetition rate and the chemical shift of that species.

Summary and Conclusions

In this paper we have demonstrated the applicability (and indeed the feasibility) of using solid-state ^{95}Mo NMR to investigate the identity of the molybdenum species on the surface of fresh catalysts. The results imply what sort of species may be present on the surface. We can identify at least four types of species that can be present on the surface of the uncalcined catalyst and at least two species present in the calcined catalyst. There seems to be at least two types of species that can interact with the surface—one that is an ordered, fully adsorbed surface species, possessing a relatively small value of Q_{cc}, and, at higher than monolayer coverage, a disordered surface species that is not fully adsorbed (i.e., it is dynamically active) but interacts with the surface.

The image that we have obtained for the surface indicates that the following species are present on the surface of the uncalcined HDS catalyst: (1) The predominant species present, independent of the pH of the method of preparation, is an ordered, adsorbed surface species possessing a relatively small quadrupole interaction. The coordination of this surface species is both tetrahedral and octahedral with the relative concentrations of each being dependent on the method of preparation. The presence of tetrahedral molybdenum species has also been corroborated by work that we have recently finished on the reduced/sulfided $Mo-Al_2O_3$ catalysts.[66] (2) At high loadings (greater than monolayer coverage), a disordered, surface-interactive, dynamic species is formed, which is chemically distinct from the adsorbed surface species. This dynamic species is adsorbed to the alumina or polymerized with the surrounding molybdenum species upon calcination. (3) We found some evidence for the intact adsorption of $[Mo_7O_{24}]^{6-}$ species onto the surface of high-loading catalysts. (4) $Al_2(MoO_4)_3$ may also be present in the uncalcined catalysts.

Upon calcination, deamination occurs and the surface interactive species decompose into MoO_3 crystallites or are adsorbed to the surface. The adsorbed octahedral and tetrahedral species are polymerized with each other, and with the MoO_3 crystallites, via condensation reactions with the surface hydroxyls. This phase is probably very similar to MoO_3 in structure. The following picture of the calcined catalysts was obtained: (a) The "MoO_3-like phase" (polymerized tetrahedral/octahedral polyoxomolybdenum species) is the predominant species present on the surface. (b) $Al_2(MoO_4)_3$ is stable to calcination and is present as a minor species. (c) No dynamically active species are observed in the calcined catalysts.

Another important finding is that there is adsorption of molybdate species in impregnation procedures involving solutions with high pH. This would not be possible if the model of the surface developing a net negative charge, which would prevent adsorption, were correct. What we have demonstrated is that when one is using an incipient wetness technique one must take into account the relative concentrations of the surface hydroxyls and the ions in solution ($[H]^+$ or $[OH]^-$ depending on the pH). Another factor that one cannot forget is the neutralizing effect that the counterions will have on the net charge buildup on the surface.

In future work we will investigate the effect of adding varied amounts of cesium, potassium, and cobalt as promotors. We have also sulfided and reduced the catalyst surfaces and have used the NMR technique to characterize the species present in the active catalyst. These results should be easier to interpret as the chemical shift range of Mo(IV) and Mo(VI) sulfur species is much larger than that of the oxo molybdates and polyoxomolybdates that we have reported here. Recently, we have successfully cross-polarized to ^{95}Mo in samples of $(NH_4)_6Mo_7O_{24}\cdot 4H_2O$ and $[(C_4H_9)_4N)]_2Mo_2O_7$.[67] This technique will facilitate an acceleration of the acquisition of even low-loading uncalcined catalyst samples (which still have surface protons available for cross-po-

(66) Edwards, J. C.; Ellis, P. D., to be submitted to *J. Am. Chem. Soc.*
(67) Edwards, J. C.; Ellis, P. D. *Magn. Reson. Chem.*, in press.

larization) and should allow us to investigate the idea of "surface islanding" of the adsorbed molybdates.

Acknowledgment. We gratefully acknowledge the partial support of this work by the National Science Foundation via awards CHE85-44272 and CHE86-11306, the National Institute of Health via Grant GM26295, and the U.S. Department of Energy via Grant DEFG84ER13296. We also acknowledge Cheryl Tolley of the Chemistry Department at the University of South Carolina, for her help in the FT-IR and laser Raman characterization of the ^{95}Mo-enriched sample of $(NH_4)_6Mo_7O_{24}\cdot 4H_2O$.

Syntheses and Spectroscopic Characterization of $(T(p\text{-}Me_2N)F_4PP)H_2$ and $(T(p\text{-}Me_2N)F_4PP)M$ Where $T(p\text{-}Me_2N)F_4PP$ Is the Dianion of *meso*-Tetrakis(*o,o,m,m*-tetrafluoro-*p*-(dimethylamino)phenyl)-porphyrin and M = Co(II), Cu(II), or Ni(II). Structures of $(T(p\text{-}Me_2N)F_4PP)Co$ and (*meso*-Tetrakis(pentafluorophenyl)porphinato)cobalt(II), $(TF_5PP)Co$

K. M. Kadish,* C. Araullo-McAdams, B. C. Han, and M. M. Franzen

Contribution from the Department of Chemistry, University of Houston, Houston, Texas 77204-5641. *Received February 20, 1990*

Abstract: The reaction of cobalt acetate with $(TF_5PP)H_2$ (where TF_5PP = the dianion of *meso*-tetrakis(pentafluorophenyl)porphyrin) leads to the formation of different metalloporphyrin products depending on solvent. In acetonitrile, $(TF_5PP)Co$ is the expected and obtained product of metalation. In contrast, the reaction between $(TF_5PP)H_2$ and cobalt acetate in dimethylformamide leads to $(T(p\text{-}Me_2N)F_4PP)Co$ where $T(p\text{-}Me_2N)F_4PP$ = the dianion of *meso*-tetrakis(*o,o,m,m*-tetrafluoro-*p*-(dimethylamino)phenyl)porphyrin. The formation of a dimethylamino-substituted complex in DMF is not unique to cobalt derivatives, and $(T(p\text{-}Me_2N)F_4PP)H_2$, $(T(p\text{-}Me_2N)F_4PP)Cu$, or $(T(p\text{-}Me_2N)F_4PP)Ni$ were synthesized from $(TF_5PP)H_2$ in almost 100% yield. Each $T(p\text{-}Me_2N)F_4PP$ complex was isolated and characterized by ^1H NMR, ^{19}F NMR, and UV–visible spectroscopy as well as by mass spectrometry. These compounds provide the first examples for substituted tetraphenylporphyrins where the four phenyl rings contain both electron-withdrawing and electron-donating substituents. The pentafluoro-substituted Co(II) derivative, $(TF_5PP)Co$, was also synthesized and spectroscopically characterized. In addition, both Co(II) porphyrins were analyzed by X-ray single-crystal diffraction. $(TF_5PP)Co$ crystallizes in the monoclinic space group $I2/c$, with a = 29.200 (13) Å, b = 6.552 (2) Å, c = 26.381 (10) Å, β = 104.13 (3)°, and Z = 4 while $(T(p\text{-}Me_2N)F_4PP)Co$ is found to crystallize in the triclinic space group $P\bar{1}$ with a = 13.638 (9) Å, b = 14.645 (8) Å, c = 16.677 (9) Å, α = 79.98 (4)°, β = 77.89 (5)°, γ = 65.92 (4)°, and Z = 2.

Introduction

The synthesis of 5,10,15,20-tetrakis(pentafluorophenyl)porphine, $(TF_5PP)H_2$, was first reported in 1969 and was followed by a number of studies on the synthesis, characterization, and chemical reactivity of the free base complex[1-6] or its metalated derivatives.[1,7-12] Recently, however, Gouterman et al.[13] demonstrated that the refluxing of $(TF_5PP)H_2$ and $AgNO_3$ in acetic acid does not result in formation of the expected $(TF_5PP)Ag$ product but rather gives a porpholactone derivative. Cu and Ni porpholactone (or porphodilactone) derivatives were also synthesized by the same method in acetic acid.[13]

N,N-Dimethylformamide (DMF) is a common solvent for metalation of a free base porphyrin,[14] and the syntheses of $(TF_5PP)Zn$, $(TF_5PP)Cu$, and $(TF_5PP)Pd$ were reported to occur without complication in this solvent.[1,9] However, as will be demonstrated in this paper, the metalation of $(TF_5PP)H_2$ in DMF is neither straightforward nor does it give the expected porphyrin products which have been reported and spectroscopically characterized over the last 20 years. Complexes of $(TF_5PP)M$ can

(1) Longo, F. R.; Finarelli, M. G.; Kim, J. B. *J. Heterocycl. Chem.* **1969**, *6*, 927.
(2) Scherz, A.; Orbach, N.; Levanon, H. *Isr. J. Chem.* **1974**, *12*, 1037.
(3) Levanon, H.; Vega, S. *J. Chem. Phys.* **1974**, *61*, 2265.
(4) Eaton, S. S.; Eaton, G. R. *J. Am. Chem. Soc.* **1977**, *99*, 1601.
(5) Kim, J. B.; Leonard, J. J.; Longo, F. R. *J. Am. Chem. Soc.* **1972**, *94*, 3986.
(6) Kampas, F. J.; Gouterman, M. *J. Lumin*, **1978**, *17*, 439.
(7) Eaton, S. S.; Eaton, G. R. *J. Am. Chem. Soc.* **1975**, *97*, 3660.
(8) Bar-Ilan, A.; Manassen, J. *J. Catal.* **1974**, *33*, 68.
(9) Spellane, P. J.; Gouterman, M.; Antipas, A.; Kim, S.; Liu, Y. C. *Inorg. Chem.* **1980**, *19*, 386.
(10) Stohl, F. V.; Shelnutt, J. A.; Granoff, B. *9th Intl. Congress Catal.* **1988**, *2*, 982.
(11) Chang, C. K.; Ebina, F. *J. Chem. Soc., Chem. Commun.* **1981**, 778.
(12) Nappa, M. J.; Tolman, C. A. *Inorg. Chem.* **1985**, *24*, 4711.
(13) Gouterman, M.; Hall, R. J.; Khalil, G.-E.; Martin, P. C.; Shankland, E. G.; Gerny, R. L. *J. Am. Chem. Soc.* **1989**, *111*, 3702.
(14) Buchler, J. W. In *The Porphyrins*; Dolphin, D., Ed.; Academic: New York, 1978; Vol. 1, p 408.

0002-7863/90/1512-8364$02.50/0